THEORETICAL INVESTIGATION OF ARCHITECTURE-DEPENDENT CALCIUM SIGNALING IN MULTICELLULAR NETWORKS

Juexuan Long

_____

A Dissertation Submitted to the Faculty of the

DEPARTMENT OF MATERIAL SCIENCE AND ENGINEERING

In Partial Fulfillment of the Requirements

For the Degree of

DOCTOR OF PHILOSOPHY

In the Graduate College

THE UNIVERSITY OF ARIZONA

2014

THE UNIVERSITY OF ARIZONA

GRADUATE COLLEGE

As members of the Dissertation Committee, we certify that we have read the dissertation prepared by Juexuan Long, titled Theoretical Investigation of Architecture-Dependent Calcium Signaling in Multicellular Network and recommend that it be accepted as fulfilling the dissertation requirement for the Degree of Doctor of Philosophy.

_____Date:08/13/2014

Pierre Deymier

_____Date:08/13/2014

Pak Kin Wong

_____Date:08/13/2014

Robert Erdmann

Final approval and acceptance of this dissertation is contingent upon the candidate's submission of the final copies of the dissertation to the Graduate College.

I hereby certify that I have read this dissertation prepared under my direction and recommend that it be accepted as fulfilling the dissertation requirement.

_____ Date: 08/13/2014

Dissertation Director: Pierre Deymier

STATEMENT BY AUTHOR

This dissertation has been submitted in partial fulfillment of the requirements for an advanced degree at the University of Arizona and is deposited in the University Library to be made available to borrowers under rules of the Library.

Brief quotations from this dissertation are allowable without special permission, provided that an accurate acknowledgement of the source is made. Requests for permission for extended quotation from or reproduction of this manuscript in whole or in part may be granted by the head of the major department or the Dean of the Graduate College when in his or her judgment the proposed use of the material is in the interests of scholarship. In all other instances, however, permission must be obtained from the author.

SIGNED: Juexuan Long

ACKNOWLEDGEMENT

I would like to express my deepest gratitude to my advisor, Dr. Pierre Deymier, for his excellent guidance, caring, patience, and providing me with an excellent atmosphere for doing research. I would like to thank Dr. Hoying for guiding my research in the past several years and helping me to develop my background in biology and physical experiments. I would like to thank Dr. Wong and Dr. Michael Junkin who provided the experiment support for this project. I would also like to thank Dr. Runge for giving me a lot good suggestions about research. Special thanks goes to Dr. Erdmann, who was willing to participate in my final defense committee.

To my friends, Ding Ding, Guanzhu and Muhan, thank you for giving me good suggestions about programming, biology science and helping me practice my oral presentation. I would also like to thank all my colleagues, who were always patient to answer my questions.

My completion of this project could not have been accomplished without the support of my husband, Ran Duan, and my dear parents. Your encouragement and endless patience when the times got rough are much appreciated and duly noted.

TABLE OF CONTENTS

TABLE OF CONTENTS-Continued

LIST OF FIGURES

LIST OF TABLES

ABSTRACT

Calcium signal can be found in many types of cell. It has been treated as a life and death signal in cell-level for triggering life at fertilization, controlling the development and differentiation of cells into specialized types, mediating the subsequent activity, and finally affecting the cell death. In tissues, intercellular calcium wave is thought to serve as a long-range signaling, affected by the cell architecture. The aim of this thesis is to provide insight into the intercellular calcium waves in multicellular complex structures subjected to mechano- or chemical-stimuli.

In the mechano-stimulated study, we combine the development of theoretical and experimental study of the propagation of calcium signals in multicellular structures composed of human endothelial cells. This analysis provides evidence for an effect of architecture on the propagation of calcium signals and the effect of single and dual stimulation on the multicellular structures. A simple model was established based on the calcium release/intake reaction and diffusion through gap junction from stimulated cell to the downstream cells. The simulation result shows similar results as what is shown in experiments.

In the chemical-stimulated model, we studied computationally the interdependence between intracellular calcium and inositol-1,4,5-trisphosphate (IP_3) pathway and cell-cell communication via gap junction. We investigate the influence of the microenvironment of cells on the frequency of intracellular calcium oscillation. The simulation result shows that the oscillation frequency of an isolated cell is lower than that of a cell embedded in a cell-chain. This phenomenon is attributed to retrograde diffusion of calcium and IP_3 originating from a widening range of cells in the chain undergoing oscillations. It further demonstrates the important influence of microenvironment on the bio-signaling propagation.

CHAPTER 1: INTRODUCTION

The structure/processing/properties/utilization paradigm, which is based on the specificity of bio-molecular and bio-cellular precursors, is the foundation of a new science and engineering of nano-bio material and systems. It is a compelling field that through manipulation of the primary amino acid sequence with modern recombinant DNA and molecular biology methods, polymeric proteins can be designed and fabricated to meet specific materials qualifications or perform a particular molecular task. However, the tissue- and developmental stage-specific gene expression give rise to some questions that WHAT are influencing gene expressions and HOW do they make it?

Researches into molecular and cellular level have provided valuable insight into solving the above questions. It is well known that cell behavior is regulated by the second messengers which are generated by thousands of external signals such as hormones, neurotransmitters, physical stimuli and so on. One of the most versatile and ubiquitous signaling messengers is the calcium ion (Ca^{2+}), which regulates many cellular processes and was reported existing in both undifferentiated (oocytes and eggs) and fully differentiated cells [1]. Moreover, an increase of free calcium in the cytoplasm has long been thought as a part of the activation response of fertilized egg [2]. Previous studies reported that a range of Ca^{2+} signaling events following fertilization has long-term effects on both gene expression and development to term [3].

As a simple ion, Ca^{2+} transmits information with a transient increase of the intracellular concentration. In tissues, intercellular calcium wave is thought to serve as a long-range signaling. Studies of signaling in multicellular networks have demonstrated that the architecture of these networks can have a significant impact on the behavior of individual cells as well as their

emerging collective behavior [4,5]. An understanding of intercellular calcium wave requires knowledge of the basic features of calcium. A brief introduction of intracellular calcium oscillations will be presented, followed by some summaries of associated mathematical models.

1.1 Intracellular Ca^{2+} Oscillation

Intracellular calcium waves were first observed in medaka eggs [6]. Subsequently, it was demonstrated existing in all cell types, as a universal signaling mode [7]. Cells display enormous oscillatory patterns that respond to different agonists [8]. In general it is possible to consider two main patterns: sinusoidal oscillations typically found in exocrine gland cells [9,10] (see Figure 1A) and transient oscillations found in endothelial cells [11] and rat chromaffin cells [12] (see Figure 1B&C). Sinusoidal oscillations are usually shown on top of an elevated level of calcium and are insensitive to changes of agonist concentration. However, transient oscillations are a series of discrete spikes rising from the resting level of calcium, which is usually sensitive to variations of agonist type and concentration.

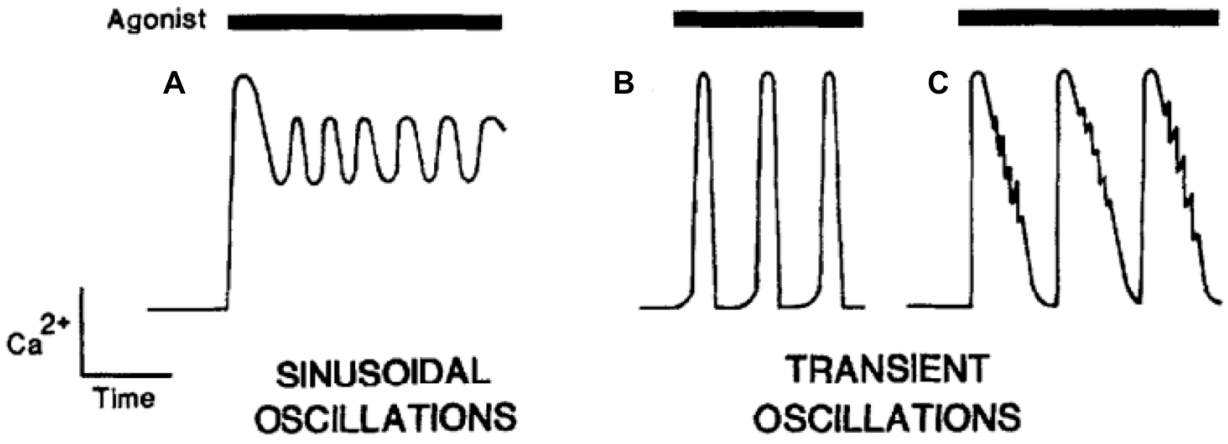

Figure 1. Typical oscillation patterns. (A) Sinusoidal oscillations. (B & C) Transient oscillations (from [19]).

Such oscillations can also be categorized into two main categories depending upon whether they originate from the extracellular space (membrane oscillators) or from the internal Ca^{2+} store such as endothelial reticulum (cytosolic oscillators) [13]. Membrane oscillator is based on the alternative opening and closing of voltage-dependent calcium channels (VOC) and various potassium channels. The opening of VOC leads to an influx of calcium, which opens the calcium-activated potassium channel to hyperpolarize the cell membrane and terminate the calcium transient. Once the potassium channel is closed, VOC is reopened due to the depolarization of cell membrane. The cytosolic oscillator depends on the periodic release of calcium from intracellular reservoirs. It reflects complex feedback interactions for intracellular calcium (see **Figure 2**).

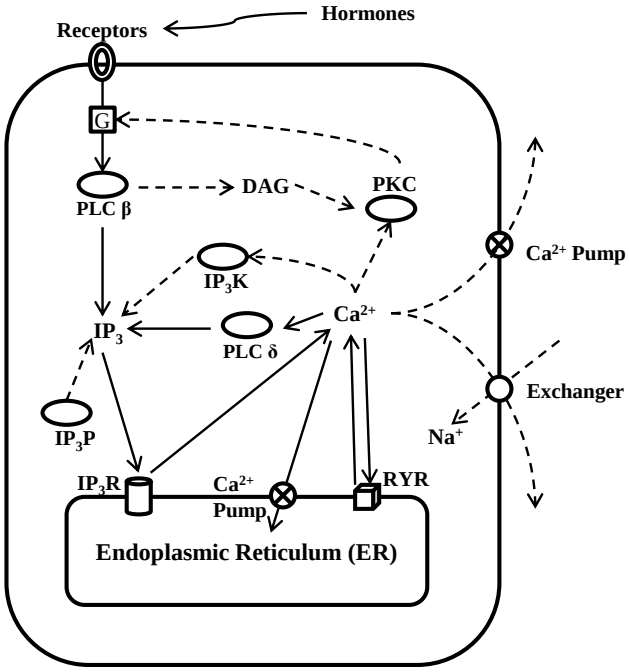

Figure 2. Schematic of intracellular calcium dynamic. The solid and dashed lines indicate the positive and negative feedback mechanisms, respectively.

It is generally regarded that the self-generation of cytosolic Ca^{2+} is controlled by the positive feedback mechanism, which consists of two pathways: the IP_3-induced Ca^{2+} release and the calcium-induced calcium release (CICR). Initially, an extracellular agonist binds with the G-protein-coupled receptors on the cell membrane to activate the phospholipase C β (PLC β). It in turn, leads to the production of inositol trisphosphate (IP_3) and diacylglycerol (DAG). In the IP_3-induced Ca^{2+} release pathway, IP_3 binds to its receptor—IP_3R and opens the calcium channel in the membrane of the ER to release the stored Ca^{2+} into the cytosol. When the intracellular Ca^{2+} concentration exceeds a threshold, PLC δ is activated and catalyzes the regeneration of IP_3, which helps to release more Ca^{2+} from ER. In the CICR pathway, Ca^{2+} is released from ER by its action on the ryanodine receptor (RYR) on the membrane of ER. RYR is sensitive to cytosolic Ca^{2+}, but insensitive to IP_3. The increase of Ca^{2+} in cytosolic induces RYR to release more calcium from ER.

The positive feedback mechanism of cytosolic Ca^{2+} is accompanied by the negative feedback condition. For example, the generation of DAG and cytosolic Ca^{2+} concentration increase activate the phosphorylation of protein kinase (PKC), which in turn is able to phosphorylate various cellular enzymes, receptors and perhaps the G protein [14]. Moreover, IP_3 is removed by phosphorylation or dephosphorylation through not only IP_3 5-phosphatase (IP_3P) but also IP_3 3-kinase (IP_3K), which is activated by Ca^{2+} [15]. Meanwhile, cytosolic Ca^{2+} is extruded from cells by Ca^{2+}-ATPase pumps and the Na^{+}-Ca^{2+} exchangers or transported back into the ER by Ca^{2+}-ATPase pumps [16]. **Figure 2** illustrates the positive and negative feedback mechanism of intracellular Ca^{2+}.

Generally, the mathematical model of calcium oscillation can be categorized into Receptor-controlled models and Second messenger-controlled models [8]. The former is based

on the various feedback mechanisms regulated oscillations in IP_3. For example, Meyer and Stryer proposed a model in 1988 showing the crosscoupling of IP_3 and Ca^{2+} [17]. In this model, IP_3 is initially induced by the extracellular stimulus to increase the concentration of cytosolic Ca^{2+}. The increase of cytosolic Ca^{2+} level, in turn, stimulates PLC to generate more IP_3. Both Ca^{2+} and IP_3 are oscillating. In contrast to Meyer's model, the intracellular calcium oscillation model without considering the periodic variation of IP_3 is called second messenger-controlled model. For example, Goldbeter et al. reported a model predicting the occurrence of the periodic Ca^{2+} spike in the absence of IP_3 oscillation [18]. In this model, calcium is released from a IP_3-sensitive store as a result of IP_3 generation induced by external stimulus. However, the subsequent rise of cytosolic Ca^{2+} is based on release of a certain amount of Ca^{2+} from an IP_3-insensitive but Ca^{2+}-sensitive store through the CICR process. Moreover, because there are two calcium stores in this model, it can be also considered as a "two pool model" [19].

1.2 Intercellular Ca^{2+} Waves

Two decades ago, Sanderson and Dirksen carried out an incisive experiment that revealed that the airway ciliary beat frequency of a stimulated cell increases after applying a brief (~ 150 ms) mechanical stimulation [20]. More importantly, the ciliary beat frequency increases in adjacent cells with a short delay and the duration of this delay is proportional to the distance of the cell from the stimulated cell [21]. By comparing the propagation speed with electrical and mechanical signal, Sanderson *et al*. got a conclusion that the increase of ciliary activity is the result of intercellular communication via gap junction.

Some subsequent experiments demonstrated that the ciliary beat frequency is increased with the increase of Ca^{2+} concentration [22,23]. With the development of camera technique,

researchers were able to capture better images of variation of cytosolic Ca^{2+} concentration (see Figure 3). When a mechanical stimulus is applied on a single airway epithelial cell, the cytosolic Ca^{2+} concentration ($[Ca^{2+}]_i$) of this stimulated cell increases and spreads out, in a wave-like manner, across the stimulated cell in all directions to the cell boundary. With a short delay, a similar Ca^{2+} wave is initiated in the adjacent cells of the stimulated cell. This cell-by-cell communication is repeated. An increase in $[Ca^{2+}]_i$ is propagated as an intercellular Ca^{2+} wave from the stimulated cell to all the surrounding cells.

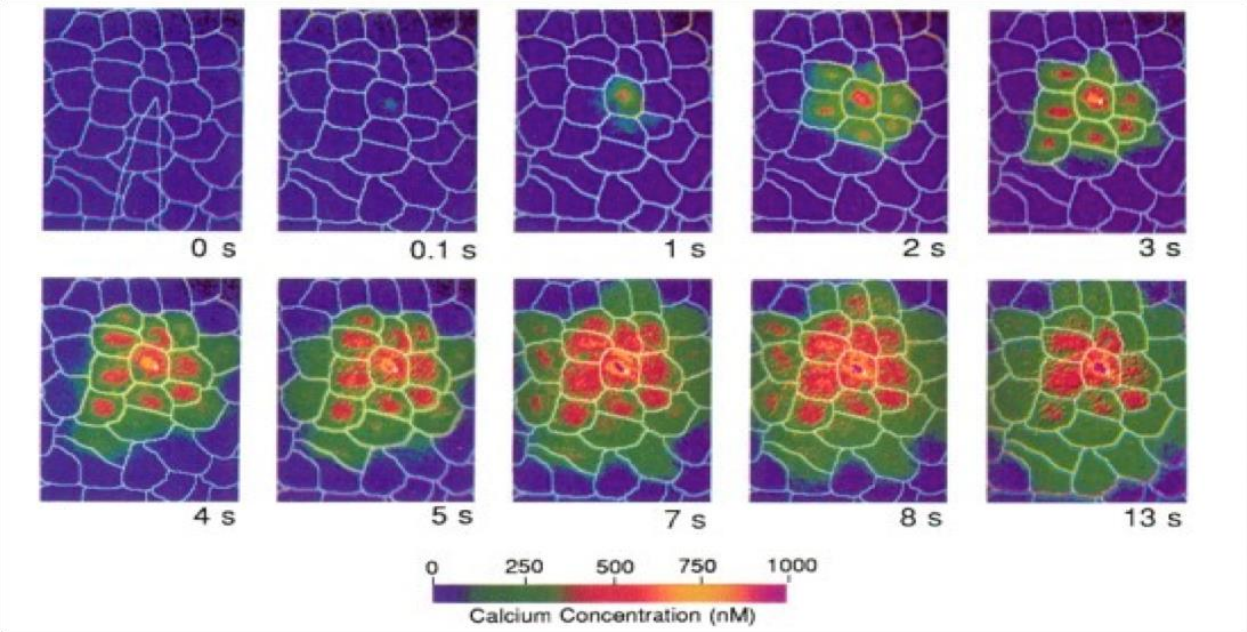

Figure 3. Intercellular calcium wave propagation in epithelial cells. (from [24])

There are two major pathways supporting the communication of signals between cells: the intercellular route with the diffusion through gap junctions and the extracellular route with the release of a diffusible messenger such as Adenosine Triphosphate (ATP) [24]. This thesis concentrates on the intercellular route based on gap junctions. Gap junction is a specialized intercellular connections. It plays a prominent role in calcium wave propagation in airway

epithelial cells [25], astrocytes [26], osteoblastic cells [27], endothelial cells [28] and so on. A dye-coupling study demonstrated that compounds of molecular masses of up to about 1000 daltons are able to permeate gap junctions [29]. Therefore, many cytosolic constituents, satisfying this property, such as Ca^{2+} and IP_3, may be allowed to pass through gap junction [30].

Sneyd et al. in 1994 proposed a model for the propagation of intercellular calcium wave [31]. The intracellular calcium dynamic in this model is based on the two-pool model. The extracellular stimulus induces the generation of IP_3 in stimulated cell and subsequently induces the calcium release from the IP_3-sensitive pool. Meanwhile, only IP_3 propagates through the gap junction to release Ca^{2+} from the IP_3-sensitive Ca^{2+} pool in the adjacent cells. In this model, intercellular Ca^{2+} fluxes are not a significant part of the Ca^{2+} wave generation. The rate of propagation of the intercellular wave only depends on the diffusion and degradation characteristics of IP_3. Permeability coefficient was introduced to control the propagation distance.

Hofer *et al.* established a famous intercellular calcium wave model in 2002 [32]. This model is based on the gap junction-dominance propagation in rat striatal astrocytes. Both Ca^{2+} and IP_3 are able to propagate from one cell to another via gap junction. Meanwhile, Ca^{2+} flux moves between the extracellular and intracellular space. Because of the effect of fast Ca^{2+} buffering, the gap-junction permeability of Ca^{2+} is set less than that of IP_3. Based on Hofer's model, Bellinger built a model taking the effect of extracellular Glu and ATP fluxes into consideration [33].

1.3 Overview of This Thesis

In chapter 2, we will present a combined theoretical and experimental study of the propagation of calcium signals in multicellular structures composed of human endothelial cells. We consider

multicellular structures composed of a single chain of cells as well as a chain of cells with a side branch, namely a "T" structure. In the experiments, we investigate the result of applying mechano-stimulation to induce signaling in the form of calcium waves along the chain and the effect of single and dual stimulation of the multicellular structure. The experimental results provide evidence of an effect of architecture on the propagation of calcium waves. Simulations based on a model of calcium-induced calcium release and cell-to-cell diffusion through gap junctions shows that the propagation of calcium waves is dependent upon the competition between intracellular calcium regulation and architecture-dependent intercellular diffusion.

In chapter 3, we develop a model-based theoretical framework to shed light on the phenomenon of cross-level interactions in complex and dynamic multicellular structures with a focus on calcium signaling via calcium waves. In particular, we investigate computationally the interdependence between intracellular calcium and inositol-1,4,5-trisphosphate (IP_3) pathway and cell-cell communication via gap junction intercellular diffusion of Ca^{2+} and IP_3. Our model shows that the dynamics of cells embedded in a multicellular network is significantly different from that of an isolated cell. In particular, we have demonstrated that the transient and steady state frequency of calcium oscillations of a cell stimulated with an agonist depends on its microenvironment, in this case, its cell neighbors. The neighborhood of the stimulated cell forms a "signaling niche" that acts on the stimulated cell itself and dynamically regulates its oscillation frequency. This effect is attributed to a crosstalk between the stimulated cell and its environment through retrograde diffusion of calcium and IP_3.

Finally, in chapter 4, we present a conclusion of major achievement of thesis and the future work we can do about architecture dependent intercellular calcium wave propagation.

CHAPTER 2. CALCIUM WAVE PROPAGATION IN NETWORKS OF ENDOTHELIAL CELLS: MODEL-BASED THEORETICAL AND EXPERIMENTAL STUDY

2.1 Introduction

Multi-level organization and dynamics is a hallmark of most biological systems. This is particularly true in tissues in which single cells are organized into multicellular structures, which are further assembled into complex tissue and organs. For example, endothelial cells are assembled into multicellular tubes (i.e. vessels), which are connected, to each other to form a branched vascular tree system. Molecular signals are initiated and/or processed at the endothelial cell level yet influence overall tree behavior and vice-versa [34]. Central to the proper behavior in these biological systems is cross-level interdependence. To date, limited studies of signaling in multicellular networks have demonstrated that the architecture of multi-cellular systems have a significant impact on the behavior of individual cells as well as their emerging collective behavior.

Over the past decade, questions concerning the system behavior of cellular structures have received increasing attention. For instance, there is strong evidence that the branching architecture of the mammary gland is a major regulator of normal epithelial cell signaling and function [4,35]. Normal organ architecture can suppress tumor formation and prevent malignant phenotypes even in grossly abnormal cells [5]. Tissue engineering in its attempt to construct functional tissues faces the challenge of arranging cells (e.g. scaffolding via decellularization of allograph tissue) in a three-dimensional configuration with architecture analogous to the native tissue to support proper spatial and temporal molecular signaling necessary to sustain appropriate

development and function [36]. Also, downstream and upstream signal conduction between endothelial cells along the walls of vessels plays an important role in microcirculatory function, vascular network remodeling, vasculogenesis, and neovascularization [37].

A particularly relevant aspect to tissue engineering is the emerging behavior of a multicellular architecture in which cell-level functions, such as intracellular communication, integrate with multicellular architectures through local cell-to-cell interactions. Central to this problem is that cellular networks inherently combine dynamical and structural complexity. Early progress on modeling coupled dynamical systems was limited to space-independent coupling or regular network topologies. Further progress to circumvent the difficulty of modeling associated with the combined complexity of the dynamics and of the architecture was achieved by taking a complementary approach where the dynamics of the network nodes is set aside and the emphasis is placed on the complexity of the network architecture [38]. Accordingly, linear solutions of calcium reaction/diffusion models of multicellular architectures composed of networks of chains of cells with grafted side branches have shown that calcium wave propagation differs in ordered or disordered architectures [39,40]. Similar effects have also been encountered in chains of endothelial cells with non-linear intracellular calcium dynamics [41].

To evaluate the effects of multilevel architectures on biological signal behavior, we modeled calcium-signal propagation in networks of endothelial cells experimentally and computationally. The vasculature is an ideal system for evaluating multi-scale behavior given the relatively simple but multi-ordered organization of the cells and tissues. Here, the behavior of a calcium wave moving along branched chains of endothelial cells was simulated using experimentally observed parameters in the computation. While there are numerous stimuli that can initiate calcium waves in endothelial cells, we utilized the mechanical stimulation of a single

endothelial cell as the wave initiator to minimize confounding issues related to multiple upstream and downstream effects intrinsic to diffusible (i.e. pharmacological) signals. Furthermore, mechanical forces play important roles in endothelial function in vivo [42]. The theoretical aspect leverages progress in modeling of the dynamics of complex networks and in microengineering of multicellular structures to generate new knowledge concerning multicellular architectures.

2.2 Methods and Model

2.2.1. Experimental method

Our study is based on networks of human umbilical vein endothelial cells (HUVEC) (ATCC CRL-1730) in which intercellular calcium wave propagation is primarily dominated by gap junction [28].

Surface Patterning

The experimental investigation of multicellular calcium ion propagation relies on organizing multiple cells into specific configurations via a surface patterning technique (Figure 4), which guided cellular attachment. Selective plasma functionalization of surfaces was employed to obtain the surface-patterning component of the system and consists of forming patterns of surface groups on biocompatible polymers [43,44,45,46,47]. The patterning is achieved via controlling contact of reactive plasma to a surface in order to spatially change surface chemistry. This process uses photolithography to first produce microscale patterns, which are designed, based on where cell attachment is desired.

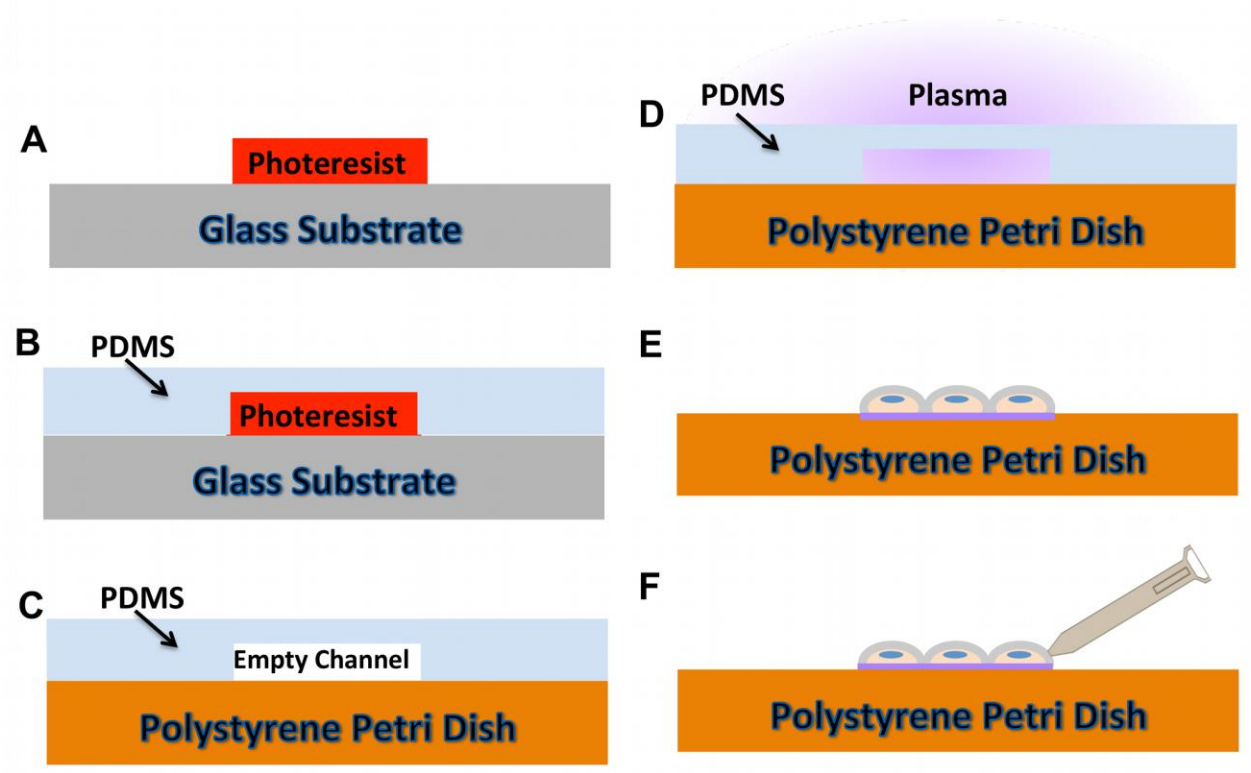

Figure 4. Plasma lithography for cell patterning. (A) Photolithography is used to form a template of the desired multicellular network. (B) PDMS is poured over the photoresist pattern to create an initial plasma shielding model. (C) PDMS mold is transformed onto a Petri Dish (polystyrene). (D) The plasma surface treatment is used to produce cell-sensitive chemical pattern on the area of PDMS mold. (E) Cell seeding. (F) Cell stimulation.

Patterning molds are then created by replica molding of polydimethylsiloxane (PDMS) onto the microscale resist structures. This produces a PDMS shape having 3D microscale topography. This 3D structure is then placed on the culture surface with a weight to ensure conformal contact and proper formation of channels between itself and the surface. The channels formed between the mold and culture surface ultimately determine where new functional groups are introduced when placed in a plasma chamber. In the case of the polystyrene substrates used in this work, select areas of native polystyrene come in contact with air plasma. This creates patterns alternating between a surface similar to tissue culture treated polystyrene, and native polystyrene, which, as it has not been modified by the plasma, is cell repulsive. For the current

experiments patterns were produced on the bottom of polystyrene Petri dishes (VWR 25384-090) using PDMS (Dow, Sylgard® 184) 3D shapes for shielding. The molds used to produce these 3D shapes were created from AZ3312 resist (AZ Electronic Materials) spun onto glass slides. The patterns were designed to be approximately one cell width wide and so had channel widths of 20-30 μm. The plasma treatment took place with air plasma for ten minutes at 150 Pa using a Harrick plasma chamber (model PDC-001) followed by ten minutes of UV sterilization before seeding with cells. Cells were detached with 0.25% trypsin-EDTA (Invitrogen), seeded onto patterned Petri dishes and incubated with standard culture medium for one day before stimulation. Standard culture medium consisted of F-12K Medium (ATCC) supplemented with 20% screened FBS (Gemini Bio-Products), 0.1 mg/ml heparin (Sigma-Aldrich), 0.035 mg/ml endothelial cell growth supplement (Sigma-Aldrich), and 0.1% gentamycin (GIBCO).

Cell Stimulation

In the current study, mechanical stimulation is used to trigger calcium release from internal stores in single cells (Figure 4(F)). We term the probed cell, "the stimulated cell", and mechanical stimulation was achieved in either of two ways (Figure 5). The first was by probing with a force sensor (FemtoTools Instruments, FT-S540), which provided a measurement of force applied to cells during stimulation. It was used to test the influence of probing force on calcium signal propagation (Figure 6). The second probing method used a 30-gage syringe needle. Since the physical size of stainless steel needle is smaller than force probe, it was used in most of our experiments including the experiments shown later to get better visualization of cells during probing compared to probing with the force probe.

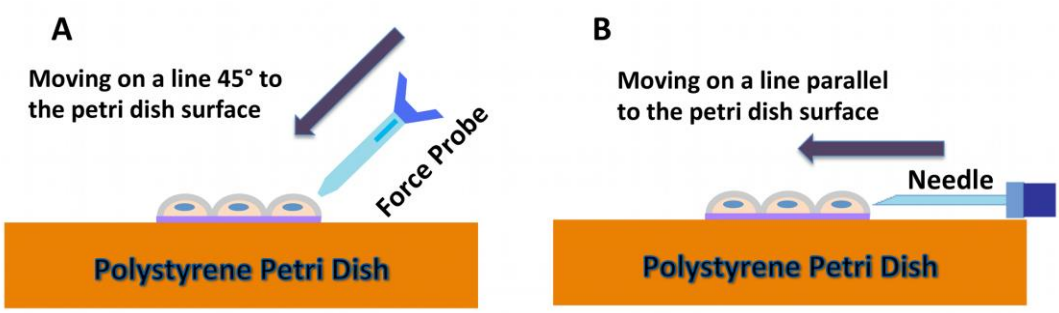

Figure 5. Schematic of cell stimulation. (A) Force probe stimulation. The direction of stimulation is from above the cells, moving 45 °to the tissue culture Petri dish surface. (B) Needle stimulation. The direction of movement is from the side, parallel to the tissue culture Petri dish surface.

The operation of the force probe required contact to a cell from above and would obscure visualization of cells adjacent to the stimulated cell. Stimulation with a syringe needle allowed the needle to be brought into contact with the stimulated cell from the side of the cell and consequently did not obscure imaging of calcium in adjacent cells. Both of these probes were attached to a custom three-axis micromanipulator for placement and stimulation. The probe would be brought near to a pattern of cells, and imaging would be initiated for baseline gathering. Fluorescence images would then continue to be captured during and after stimulation.

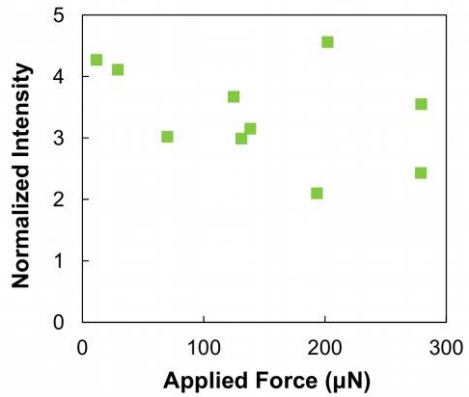

Figure 6. Influence of probing force on calcium signal intensity. A capacitive force probe (Nanoscience Inc) was applied for mechanical stimulation of individual HUVECs. The intensity of fluorescence produced by the stimulated cell shows only very weak correlation with the applied force (The R square value is determined to be 0.1667 by linear regression analysis).

Imaging

Fluro-3AM was loaded into cells as a Ca^{2+} sensitive dye to visualize the small messenger signaling. Once loaded, esterases cleave the dye so that it cannot leave the cell and will fluoresce in the presence of Ca^{2+}. A Nikon TE2000-U inverted phase contrast and fluorescence microscope equipped with a Cooke SensiCam was used to capture the images. Cells were first plated on patterned surfaces as described above and maintained in standard culture medium. Dye loading was initiated by adding 5 or 10 µl of a 1 mg/ml solution of Fluo-3AM (Invitrogen) dissolved in dimethyl sulfoxide (DMSO), (Fisher) and 5 or 10 µl of a 10 mg/ml solution of Pluronic® F-127 (Invitrogen) dissolved in deionized water, to the three milliliters of standard culture medium contained in the patterned dish. The cells were then incubated for 15 minutes at 37℃ before being gently rinsed with standard culture medium. New culture medium was added and the cells were incubated for ten minutes at 37℃. Medium was then exchanged and cells were incubated for another ten minutes at 37℃. Finally cells were rinsed with HBSS without calcium or magnesium (Fisher) and the same HBSS was added for imaging, which took place on a microscope stage heated to 37 ℃. Prior to stimulation, images were captured in phase contrast to visualize cell outlines and during stimulation, illumination was changed to fluorescence with a filter cube providing excitation at 460-500 nm and emission at 510-560 nm. Images were captured every 1.2 seconds and exported for later analysis. For analysis, cells were manually outlined in image sequences and analyzed using Image J, which exported integrated fluorescence versus time values for later analysis. Images and probing were obtained within ~25 minute of the final buffer rinse and cells were imaged at passage six or lower.

Whole cell fluorescence intensities as a function of time are obtained by integrating the intensity of every pixel over the area of each cell corrected for the integrated fluorescence of a

background area and normalized by the initial intensity. In absence of a one-to-one correspondence between normalized fluorescence intensity and the level of cytosolic calcium concentration, and in light of the cell-to-cell variability in the intensity of the fluorescence, the magnitude of fluorescence is not always taken as a measure of the response of a cell. Irrespective of the magnitude of the fluorescence, a cell is considered to have responded when it exhibits a temporal fluorescence response constituted of an initial fast rising stage followed by a slower decline in fluorescence (see section "2.3.1-Chain Subjected to Single Stimulation: Experiments" for details). The response time of a cell is then determined as the time at which fluorescence reaches its maximum positive rate of change. For weak temporal responses that exhibit significant noise levels, the noise to signal ratio is improved by calculating the running average of the rate of change of the fluorescence. The time average is performed on four time intervals. Response times determined from the running average will therefore be associated with larger uncertainties of 1.2 s.

2.2.2. Computational model and method

Since we are interested in the behavior of networks of endothelial cells composed of one-dimensional chains of cells and networks of chains of cells, a reaction/diffusion model is developed to gain insight into the architecture-dependence of calcium wave propagation. For the sake of simplicity, we only consider the dynamic of intracellular calcium and assume the intercellular Ca^{2+} is transported between cells by diffusion through gap junctions.

Numerical Model

The model is based on the one-dimensional time-dependent reaction/diffusion equation:

$$\frac{\partial C}{\partial t} = D\frac{\partial^2 C}{\partial x^2} + f(C) \quad (2\text{-}1)$$

where *C* is the cytosolic calcium concentration, *D* is a coefficient representing diffusion between cells through gap junctions, and *f* is the rate of change of intracellular calcium concentration. *x* and *t* are the position and time variables.

Intracellular calcium dynamics results from the response of Ca^{2+} stores, primarily the endoplasmic reticulum (ER), to inositol triphosphate (IP_3) and ryanodine through IP_3 receptors (IP_3R) [48] and ryanodine receptors [49]. Both sensitized IP_3R and RYR, lead to a process whereby calcium can trigger the release of additional calcium from the ER, namely calcium induced calcium release (CICR). Furthermore, since high levels of intracellular calcium are toxic, and cannot be degraded, cells control the intracellular calcium level by buffering, sequestration in specialized compartments, and by expulsion to the extracellular space [50]. Meanwhile, cytosolic calcium concentration is also inhibited by low level of Ca^{2+} [48,51]. In the basis of these processes, we model the rate of change of intracellular calcium by a simple calcium dependent non-linear reaction function:

$$f(C) = -k(C) * C \quad (2\text{-}2)$$

with $k(C)$ representing a calcium concentration-dependent calcium release/intake rate constant. To model the CICR and calcium buffering processes, we defined two thresholds UC_1 and UC_2, which determine the value of the calcium release/intake rate as shown in Figure 7.

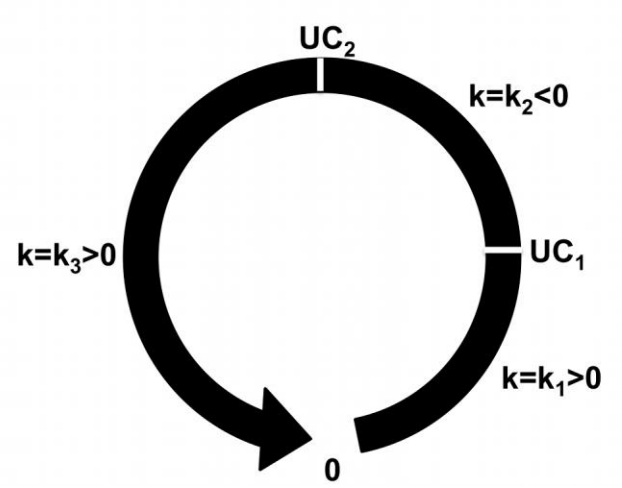

Figure 7. Schematic representation of the non-linear intracellular calcium reaction dynamics as a loop in calcium concentration space. *UC1* and *UC2* are lower and upper thresholds of intracellular calcium concentration, respectively, which determine the value of calcium release/intake rate constant, k.

UC1 is the threshold below which cytosolic calcium concentration is too low to promote ER release of additional calcium. Therefore, for calcium concentrations below *UC1*, the ER absorbs cytosolic calcium and the calcium release/intake rate constant takes on a positive value $k(C)=k_1$. The rate of calcium dynamics, *f*, is therefore negative which corresponds to ER calcium intake. Calcium is released from ER to the cytosol, when the cytosolic calcium concentration is within the range *UC1* and *UC2*. Within this range, the value of the calcium release/intake rate constant, $k(C)=k_2$ is negative and *f* is positive. This corresponds to release of calcium by the ER and the total concentration of cytosolic calcium increases. If the intracellular calcium level exceeds the threshold *UC2*, then the cytosolic calcium is again absorbed into ER or extruded to extracellular space. Within this range, the value of the calcium rate constant, $k(C)=k_3$ is positive and the rate of the cytosolic calcium dynamics is negative. Because cells exhibit a refractory stage of approximately 30 s after a complete cycle of calcium release followed by intake [32], in our model once the calcium rate constant reaches the value k_3, the cell will retain that value indefinitely.

In the case of a spatially discrete representation of multicellular chain and considering diffusion between nearest neighbor only, equation (1) is discretized in space and time using finite differences and takes the form:

$$C(x_i, t_{n+1}) = C(x_i, t_n) + D^*[C(x_{i+1}, t_n) - 2C(x_i, t_n) + C(x_{i-1}, t_n)] - k^*(C)C \qquad (2\text{-}3)$$

The term on the left-hand side is the concentration of Ca^{2+} in cell "*i*" at time t_{n+1}, and all the terms on the right-hand side are at a time t_n. The time step is denoted Δt. The concentration for the next time increment, *n+1*, can be calculated from values of concentration at the previous time increment, *n*. $\frac{D*\Delta t}{(\Delta x)^2}$ is defined as a dimensionless diffusion coefficient denoted "*D**". $k^*(C) = k(C)\Delta t$ represents a dimensionless rate constant. For linear chains of endothelial cells, we assume that the calcium diffusion coefficient is the same between neighboring cells. However, we will consider spatially dependent diffusion coefficients in the case of models of more complex architectures such as "T" structures. This more complex model is detailed in the Appendix I. Calcium signals described by our model do not exhibit attenuation since we observed variations in the fluorescence intensity in individual experiments. Nevertheless, our model is able to capture the major features of intercellular calcium propagation described in the paper (see Figure 8).

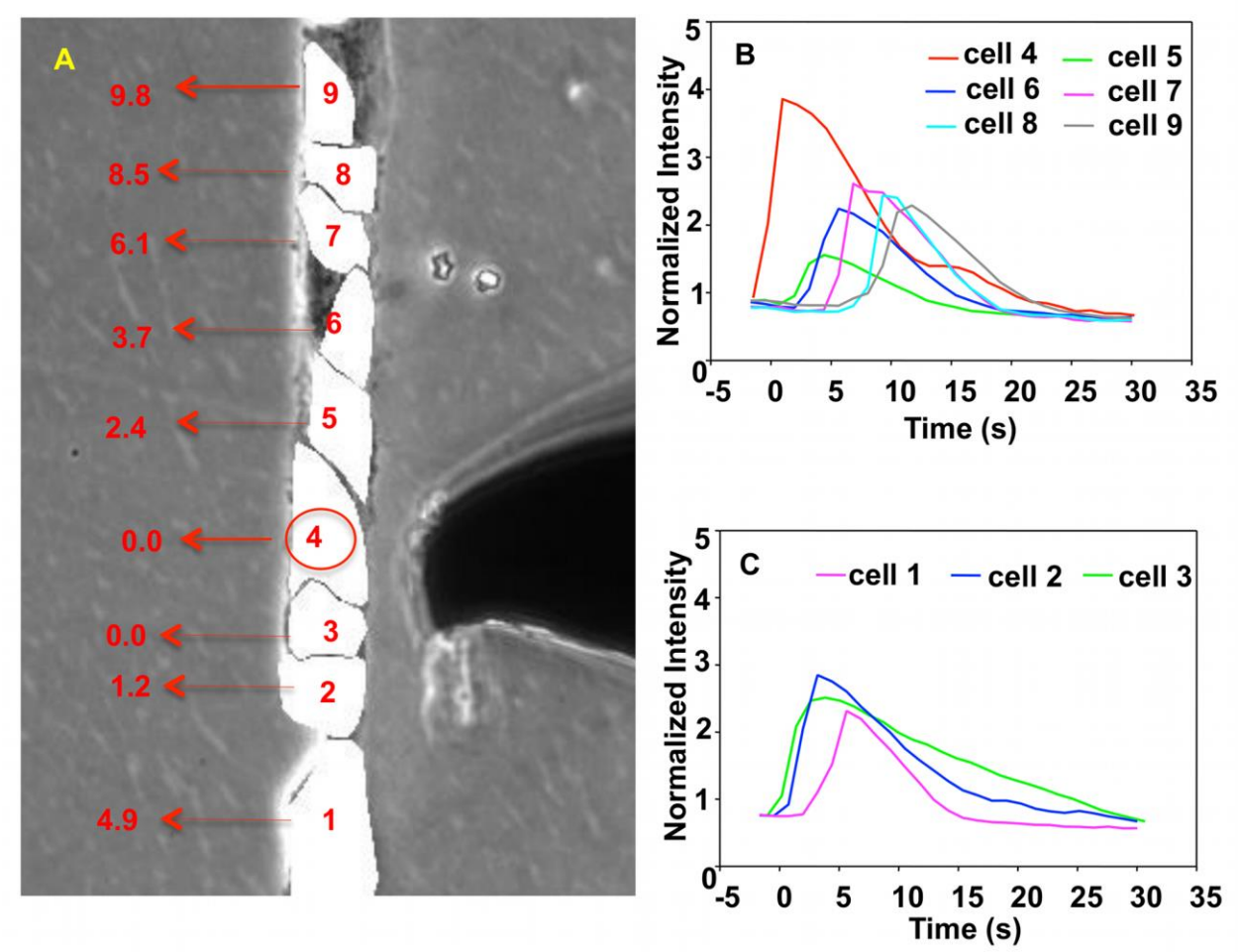

Figure 8. Experiment image and normalized intensity of cells in single fine line subjected to single stimulus. (A) Image of a finite single fine line of cells. Cells are labeled 1 through 9. The stimulating probe is clearly visible on the right of the stimulated cell (cell 4 labeled with a red circle). The time (in sec) at which the normalized fluorescence reaches its maximum positive rate of change is indicated for every cell. The uncertainty for each one of these times is 0.6 sec. The origin of time is the time at which fluorescence in the stimulated cell attains its maximum rate of change. (B) and (C) show the normalized intensity of fluorescence of cells 4 through 9 and cells 3 through 1, respectively, as functions of time. The vertical axis is the dimensionless normalized intensity of fluorescence and the horizontal axis is the time in seconds in intervals of 1.2 s between recordings.

2.3 Result and Discussion

We investigate the behavior of several types of multicellular structures, namely single chains of endothelial cells and "T" structures subjected to either single or simultaneous double mechano-stimulation at different locations in the structures.

2.3.1 Chain subjected to single stimulation

In this section we consider the behavior of a finite chain of endothelial cells among which a single cell in the chain is subjected to mechanical stimulation to initiate a calcium impulse, due to the intracellular increase in calcium concentration.

Chain Subjected to Single Stimulation: Experiments

Figure 8 shows the calcium-activated fluorescence of individual cells as a function of time in a finite single fine line of cells with one cell (cell 4) subjected to a single mechano-stimulation. Note that since the fluorescence of the system is recorded every 1.2 s, the response time of every cell in the structure is associated with an uncertainty of 0.6 s.

The observed shape of the calcium pulse is consistent with that previously reported [52]. While we observed some attenuation of the pulse amplitude as a function of distance in several cases as reported by others [32], this did not occur in all experiments (as in Figure 8). The response time of a cell is defined to be the time corresponding to the highest value of the rate of change of fluorescence versus time. The response time of the stimulated cell (cell 4) is set as the origin of time. The response of cells 5 through 9 and 3 through 1 lags behind that of the stimulated cell as an increasing function of the distance from the stimulated cell. Thus two calcium pulses propagate along the cell chain in opposite directions with both pulses originating at cell 4. Figure 8 indicates that calcium pulses can propagate over distances of at least 3 to 5 cells

with relatively high intensity beyond the stimulated cell. For 20 different cell chains we examined, calcium pulses propagated from the stimulated cell with an average distance of propagation of 4.7 cells with a standard deviation of 1.1. Furthermore, the degree of force applied (from 3 to 300 μN) to the cell had no significant effect on the distance of propagation of a calcium pulse (Figure 6). This indicates that the propagation of the calcium pulse over a finite distance is not driven by stress/strain induced effects along the chain of cells. Also the normalized fluorescence intensity appears to be independent of the force applied. Based on the experimental data shown in Figure 8, the average time of the propagation of calcium wave from one cell to the next is approximately 1.8 s. Moreover, the average width of a temporal pulse is on the order of 10 to 15 second. This means that a regular pulse may extend spatially over 6 (10/1.8) to 9 (15/1.8) intercellular spacing. The average distance between cells in a single chain is approximately 31.2 μm. Therefore the average speed of a calcium wave is estimated to be on the order of 17 μm/s. It is important to note that the time it takes for the fluorescence signal to propagate from cell to cell is highly variable, differing by a factor of two in some cases. The variation may be due to the variability in cell size, cell state, gap-junction distribution in the cell membrane, or other characteristics of the cells.

Chain Subjected to Single Stimulation: Simulation

The cell chain in the simulation consists of 61 cells aligned in single fine line. To begin the simulation, a pulse is initiated in the middle-most cell of the chain, which is sufficiently far from the edges of the chain to avoid artifacts that could arise from boundary effects. For the ease of comparison with the experimental results, we subsequently label the cells in the chain from 26 through 34 such that the stimulated cell is labeled as cell 4. The initial calcium concentration of all but the stimulated cell is set to zero. The initial calcium concentration of the stimulated cell is

C_0, which is greater than UC_1. This initial concentration triggers the CICR process initiating a pulse. The value of the model's parameters was explored with consideration of three criterions: (1) the set of parameter values should ensure the propagation of intercellular calcium wave along the cell chain; (2) the parameter values should mimic the two-stage calcium pulses shown in experiments: an initial fast rising calcium concentration followed by a slower decrease with pulse spatial extension of 6 to 9 intercellular spacing; (3) the dimensionless diffusion coefficient should correlate with a reported real diffusion coefficient. To satisfy the criterion #1, we derive a set of parameter value initially via trial and error (shown in Table 1).

Table 1. First set of Value of dimensionless parameters

Symbol	Definition	Value
C_0	Initial concentration of calcium in stimulated cell	0.5
UC_1	Calcium concentration threshold 1	0.3
UC_2	Calcium concentration threshold 2	1.2
k_1^*	Calcium release/intake rate for $C< UC_1$	1.0
k_2^*	Calcium release/intake rate for $UC_1<C< UC_2$	-1.0
k_3^*	Calcium release/intake rate for $C>UC_2$	0.25
Δt	Time interval	0.01
D^*	Dimensionless diffusion coefficient	0.7

Based on the parameter value listed in Table 1, we explore the influence of diffusion coefficient on the intercellular calcium propagation. We modify the value of D^* without changing the value of other parameters. The intercellular calcium propagation only occurs when the value of D^* is in [0.62, 0.74] named effective interval. If the value of D^* is beyond this range, there is no calcium signal propagating along the chain. When $D^*<0.62$, the inward fluxes are not larger than the rate of decrease of calcium concentration in the non-stimulated cells. Cells are unable to accumulate enough Ca^{2+} to trigger CICR. Calcium pulses, therefore, will not propagate along cell chain. When the $D^*>0.74$, the outward diffusion fluxes are too large to help the accumulation of intracellular calcium. Therefore, intercellular calcium wave propagation will not occur neither.

However, the length of the effective interval of D^* is not rigid. It depends upon the value of other parameters. Table 2 lists the relation between the effective interval of D^* and the value of UC_2 that determines the capacity of cells for cytosolic calcium concentration. We can see that the increase of the cell's capacity is able to support the intercellular calcium wave propagation at lower diffusion coefficients. Because the increase of cell's capacity prolongs the time of positive intracellular calcium dynamic (period of CICR), the neighboring cells have more time to accumulate enough Ca^{2+} to exceed the threshold UC_1. Moreover, diminishing the value of UC_1 can also decrease the lower bound of the effective interval of D^*. Meanwhile, we notice that the upper bound of effective interval is insensitive of the value of threshold including both UC_1 and UC_2, but has positive correlation with the rate of increase of intracellular calcium, k_2^* (data not shown).

Table 2. Relations between UC_2 and the lower bound and upper bound of effective interval of D^*

UC_2	Lower Bound of D^*	Upper Bound of D^*
1.5	0.44	0.74
2.0	0.3	0.74
2.5	0.23	0.74
3.0	0.18	0.74
3.5	0.15	0.74

We also investigate the range of concentration between UC_1 and UC_2, over which calcium signal is propagating along the chain. **Figure 9** illustrates the relationship between UC_1 and UC_2 without changing the value of other parameter shown in Table 1. The increase of UC_1 asks for a more rapid increase of UC_2 to meet the demand of criterion #1. This may due to influence of calcium concentration gradients. The higher threshold UC_1 requests a larger gradients existing between two neighboring cell which can be achieved by increasing the calcium concentration capacity of cells.

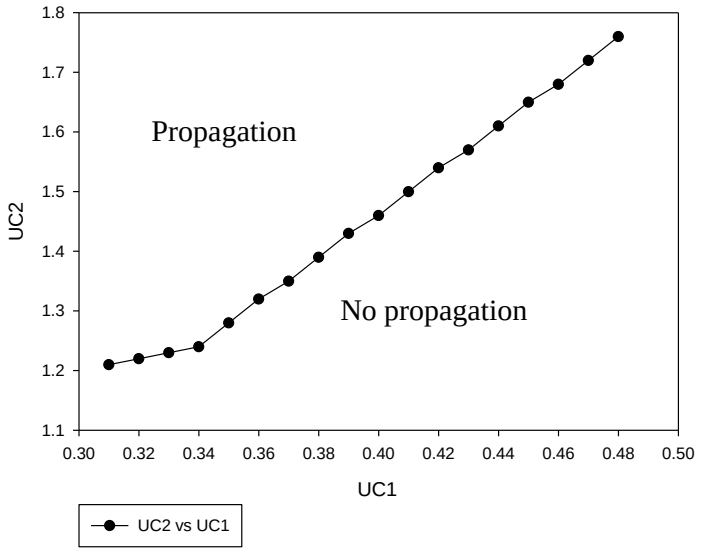

Figure 9. Relationship between UC_1 and UC_2. The region above the line contains the values of UC_1 and UC_2 which support the intercellular calcium wave propagation. The region below the line stands for the values that stop the intercellular calcium wave propagation.

Besides UC_1, UC_2 and D^*, the other parameters also play an important role in forming calcium pulses. For example, the value of k_1^* determines the difficulty for cells to exceed the threshold UC_1; k_2^* is the rate of CICR determining the time cells have to take to reach the maximum intracellular calcium concentration; k_3^* controls the speed of decline of calcium concentration when the concentration exceeds the UC_2.

Based on the study introduced above, we explore the value of each parameter until system exhibits calcium wave propagation with characteristics comparable to those of the experimentally observed wave. In particular, we search for parameters that satisfy the criterion #2. The parameter value used in our model is listed in Table 3. The simulated calcium pulse has a spatial extend of approximately 10 cells comparable to what was observed experimentally.

Table 3. Value of dimensionless parameters used in the reaction-diffusion model of intercellular and intracellular reaction-diffusion dynamics

Symbol	Definition	Value
C_0	Initial concentration of calcium in stimulated cell	2.0
UC_1	Calcium concentration threshold 1	0.3
UC_2	Calcium concentration threshold 2	3.0
k_1^*	Calcium release/intake rate for $C< UC_1$	0.03
k_2^*	Calcium release/intake rate for $UC_1<C< UC_2$	-0.025
k_3^*	Calcium release/intake rate for $C>UC_2$	0.0045
Δt	Time interval	0.01
D*	Diffusion coefficient	0.6

In the model all rates are dimensionless. The evolution of the calculated calcium concentration in each cell is reported in **Figure 10**.

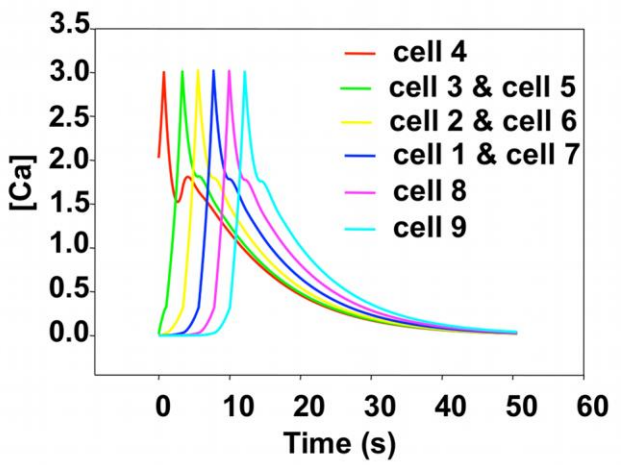

Figure 10. Simulated calcium concentration for cells in a single chain subjected to a single stimulus. We label the stimulated cell 4 (cell 31 in the chain of 61 cells). We report the response of cells on either side of the stimulated cell as cell 5 through cell 9 and cell 1-through cell 3 to facilitate comparison with experimental results. The real time is obtained by scaling the cell-to-cell propagation time of the simulation to that of the experiment (see text for details).

From the experimental data, the average time for propagation from one cell to the next one is 1.8 s. In the simulation, the dimensionless time for propagation from one cell position to the next one is 0.87. Thus, we obtain a conversion factor from dimensionless to real time, $\tau = \frac{1.8\,s}{0.87} = 2.07\text{s}$. Therefore, the dimensionless integration time step $\Delta t=0.01$effectively amounts to 0.0207 s. With an average experimental spacing between cells of L=3.12x10^{-5} m and a dimensionless diffusion coefficient in the simulation of D^*=0.6, we can calculate the actual value of the diffusion coefficient in our model as $D = D^* \times \frac{L^2}{\tau} = 7.84 \times 10^{-10}\ (\text{m}^2/\text{s})$. Note that this diffusion coefficient accounts for calcium diffusion between cells through the cytoplasm as well as through gaps junctions. It is in reasonable agreement (in the same order of magnitude) with a free Ca^{2+} diffusion coefficient in a cytosolic extracts from *Xenopus laevis* oocytes of 2.2×10^{-10} m^2/s [53].

Propagation is symmetric in the simulation and the response of cells 5 and 3, cells 6 and 2, cells 7 and 1 are the same. There is no variability in the magnitude of the calcium response from cell to cell in the model. The development of a calcium wave that propagates on both sides of the stimulated cell results from the competition between intracellular dynamics and intercellular diffusion. The calcium concentration of the stimulated cell initially exceeding UC_1 leads to ER calcium release and therefore a fast rise in the cytosolic calcium in spite of a competition with diffusion that leaks calcium to the neighboring cells. When the concentration of cell 4 exceeds UC_2 it declines steadily. Diffusion from cell 4 to cells 3 and 5 increases their respective calcium concentration beyond UC_1, which in turns triggers CICR. This process sustains the propagation of a calcium wave. Note that in the simulation, there is a smaller hump appearing in the tail of each pulse. This behavior, which has no significant effect on the simulation result, is not observed experimentally and is an artifact resulting from the discrete nature of the model. Indeed calcium diffusion is bi-directional and driven by the calcium concentration gradient between neighboring cells. When the calcium concentration level in cells 5 and 3 reaches its highest level, the calcium concentration in cell 4, which is in a declining phase can rise again due to a large calcium diffusion flux originating in cells 5 and 3. This behavior would be more diffuse in a model that would account for the continuous nature of the cell cytoplasm.

2.3.2 Double stimulation of single chain

We now consider the behavior of a chain of cells subjected to dual mechano-stimulation. The stimulations are applied simultaneously on two cells separated by a short distance. In light of an average distance of propagation of a calcium pulse of approximately 4.7 cells, this distance is chosen so that one could expect possible overlap of the signals emanating from the two stimulated cells in the region separating them.

Single Chain-Dual Stimulation: Experiment

Figure **11** shows one example of a chain of endothelial cells with dual stimulation. Here, the stimulated cells are separated by 6 cells, which is shorter than two times the average distance of propagation of calcium pulses.

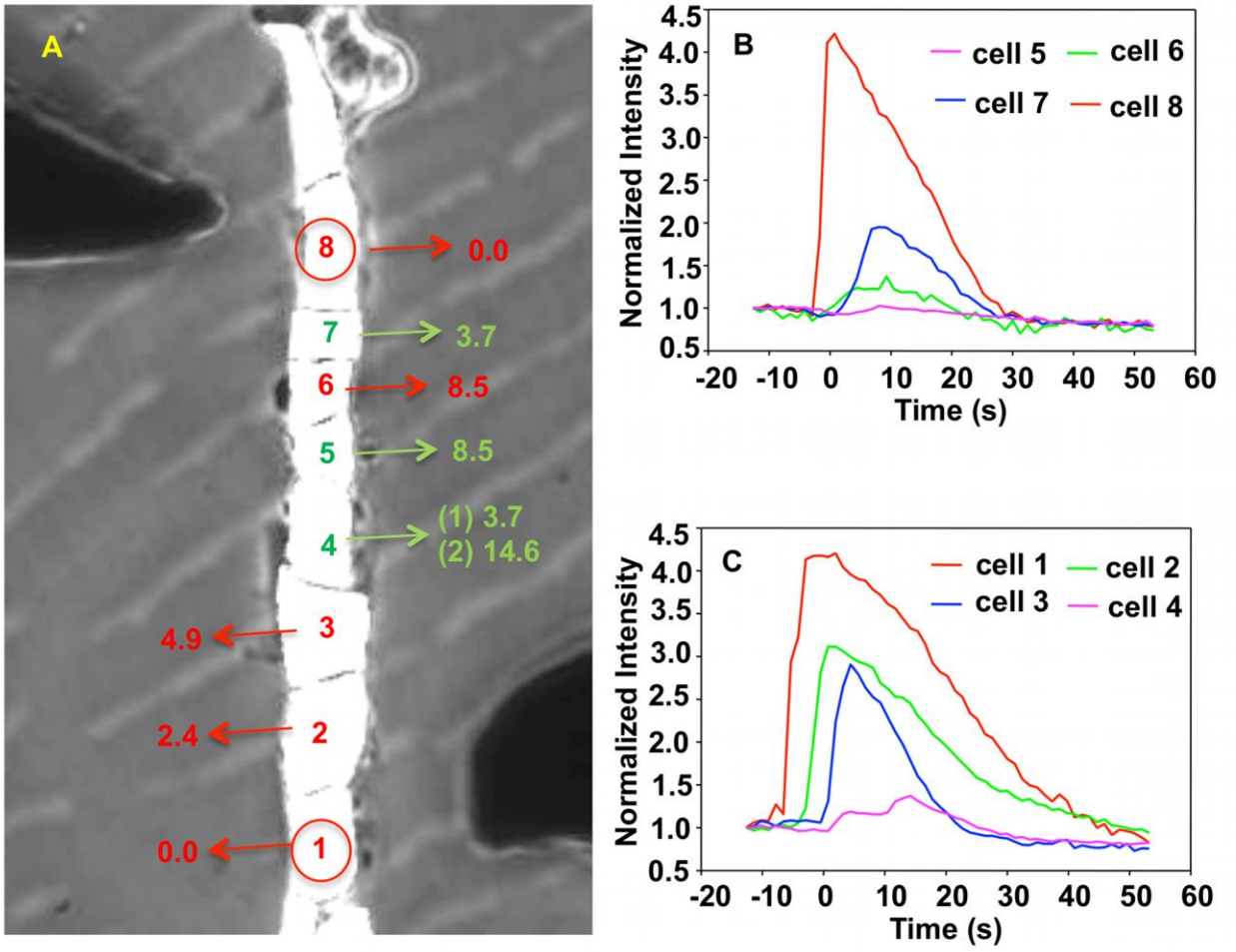

Figure 11. Experiment image and normalized intensity of cells in single fine line subjected to double stimulus. (A) Image of a finite single fine line of cells subjected to dual mechano-stimulation. The stimulating probes are visible at the top-left and bottom-right of the image. The response time of cells labeled in red was calculated from the maximum rate of change of the fluorescence intensity with uncertainties 0.6 s. The response time of cells labeled in green was calculated from a running average of the fluorescence intensity with uncertainties 1.2 s. The first response time for cell 4 (1), represents the time of the first sharp rise in fluorescence versus time. The second response time of cell 4 (2) indicates the time when the fluorescence intensity

increases a second time. Cells 4 and 5 represent the region where the calcium pulses are anticipated to meet. (B) and (C) present the normalized intensity of fluorescence of individual cells as a function of time.

The time evolution of the fluorescence intensity of cells 4 and 5 is significantly different from that of the other cells and of signals observed in the case of a single chain with a single stimulation. As stated in section "2.2.1-Imaging", the determination of the cell response time from signals with weak intensity is conducted on a running average of the rate of change of the intensity.

In Figure **11**(A), the average time for propagation from one cell to a neighbor of a pulse originating at cell 8 is $t_d \approx 2.8$ s (the subscript "d" stands for downward propagation), and the average cell-to-cell propagation time of a calcium pulse originating at cell 1 is $t_u \approx 1.6$ s (the subscript "u" stands for upward propagation). The statistical average times for propagation from one cell to next one based on averaging 17 experimental samples are $t_d \approx 3.81$ s with standard deviation *STDEV*=2.32 s and $t_u \approx 3.84$ s with standard deviation *STDEV*=2.11 s. Calcium signals can propagate over an average maximum distance of 5 to 6 cells following a single stimulation event. Because of the difference in upward and downward cell-to-cell propagation time, and considering the possibility of calcium signals that could cross, one would expect to observe a second peak in the response of cell 3 at approximately 17 s, however, this is not the case. The absence of this second peak indicates that once the first pulse has triggered CICR of cell 3, that cell is unable to respond a second time in less than 17 s. This is a characteristic of the refractory behavior of a cell. However, cell 4 appears to exhibit a second peak. This cell is therefore the location where the two pulses meet with a time difference of approximately 10 s. The absence of a second peak in the response of cells 5 and 6 supports this inference. These observations indicate that the two pulses, which propagate toward each other, are unable to pass

each other due to the refractory behavior of CICR in endothelial cells. We conducted 26 experiments similar to that reported in Figure **11** and 25 out of 26 of these showed calcium pulses that are not able to cross one another. This result provides strong statistical evidence for the absence of calcium wave crossing in chains of endothelial cells.

Single Chain-Dual Stimulation: Simulation

As described in section "2.3.1-Chain Subjected to Single Stimulation: Simulations", we simulated the behavior of a long chain of cells by modeling a chain with sufficient length to avoid any edge effect during the simulation time when the dual stimulation is applied in its central region, namely cells 1 and 8. All initial calcium concentrations are set to zero except for the stimulated cells, which have an initial calcium concentration exceeding the threshold UC_1. The cells located between the stimulated cells are labeled cells 2 through 7. Due to the symmetry of the model, cells 1 and 8, 2 and 7, 3 and 6, 4 and 5 behave in exactly the same way (See Figure **12**).

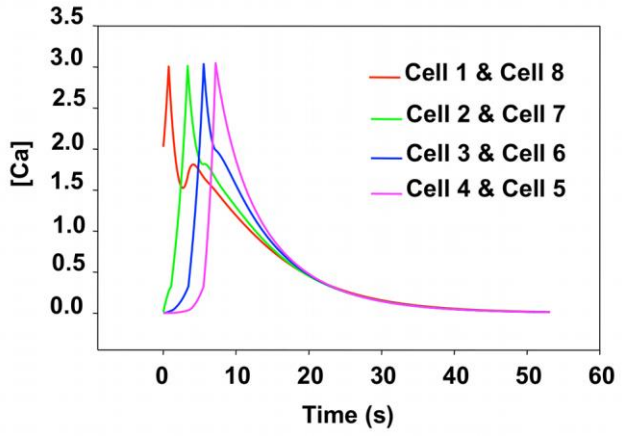

Figure 12. Simulated calcium concentration for cells in a single chain subjected to double stimulus. Cell 1 and cell 8 are the stimulated cells. We report the response of cells between the stimulated cells as cell 2 through cell 7 to facilitate comparison with experimental results. The real time is obtained by scaling the cell-to-cell propagation time of the simulation to that of the experiment (see text for details).

The response of cell 1 and 8 shows a secondary peak already attributed to the discrete nature of diffusion in our model. If the calcium pulses propagating in the segment between cells 1 to 8 were able to cross one would expect a peak in calcium concentration of cell 1 resulting from the pulse originating at cell 8 at an approximate time of 16 s. The response of cell 1 does not show such a peak. The occurrence of such a peak is not possible since the computational model includes implicitly a refractory stage for CICR. The calcium waves originating from the stimulated cells merge at cells 5 and 4. There, the calcium concentration decays steadily as the rate of calcium dynamics is negative and further response of the cells is prevented. In other words, once the rate of intracellular calcium dynamics, k_3^*, is reached, a cell cannot respond anymore and the calcium pulses do not cross, as observed in the experimental and computational findings.

2.3.3 "T" structure subjected to single stimulation

The growth of "T" structures formed by surface-patterning perpendicular single chains of cells does not permit the formation of cellular junctions composed of a single cell. Typically, many cells aggregate at the junction of the three branches forming a cell cluster (see **Figure 13** and Figure **14**).

"T" Structure-Single Stimulation: Experimental

In this "T" structure, a single stimulation was applied to one of the branches to determine if the calcium signal can propagate through the junction area and trigger a signal in both of the other branches. We illustrate in Figure **13** and Figure **14** the behavior of "T" structures with two cases. In both cases, the stimulated cell is located in the lower branch (branch 1) at the edge of

the junction area. This is done to ensure that there exist paths for the propagation of a calcium pulse to the other branches that do not exceed 4 to 5 cells in length.

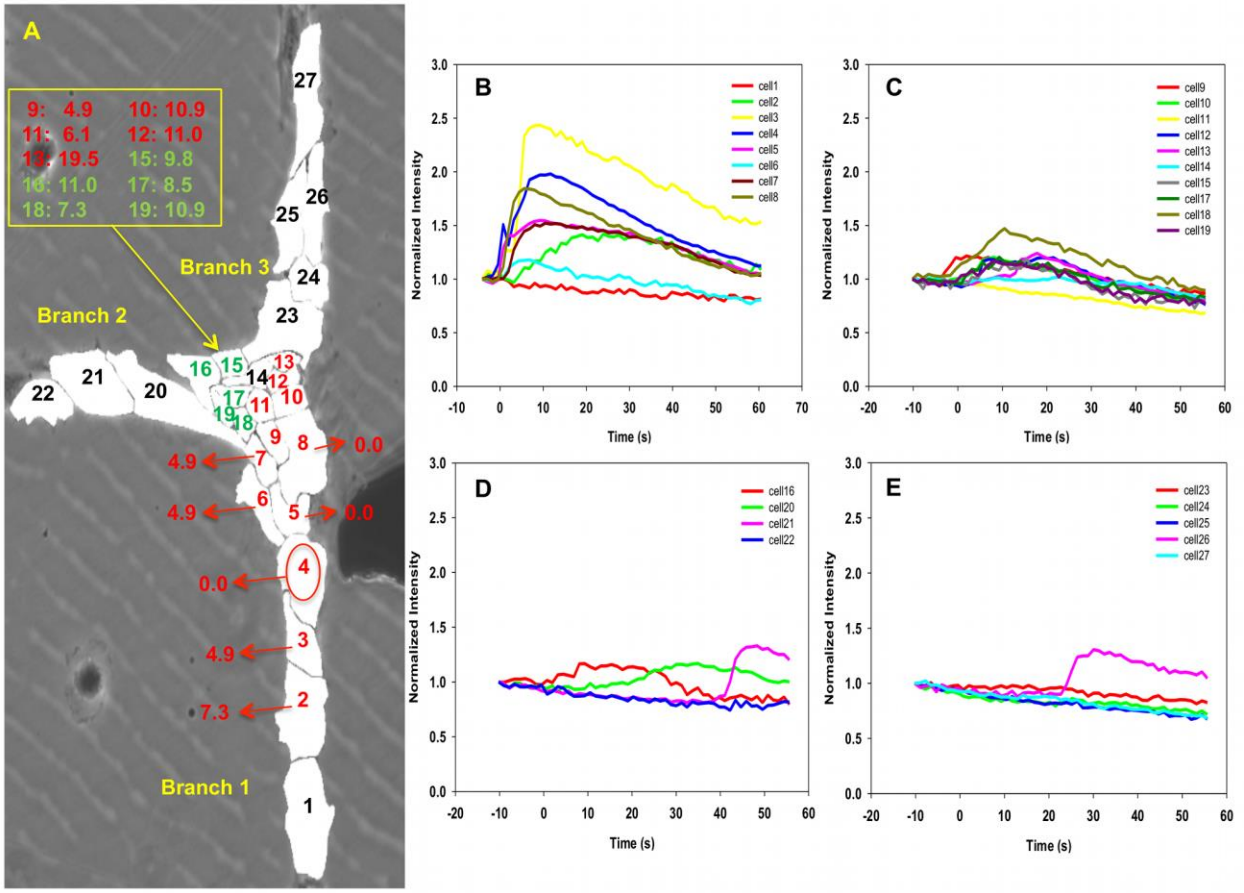

Figure 13. Experiment image 1 and normalized intensity of cells in "T" structure subjected to a single mechano-stimulation. (A) Image of a T structure of cells subjected to single mechano-stimulation. The red circle indicates the location of the stimulated cell. Red labels correspond to cells exhibiting strong fluorescence with response time measured from the rate of change of the fluorescence intensity. Green labels correspond to cells exhibiting weak fluorescence and response time derived from running averages of the rate of change of the fluorescence intensity. Black labels are for cells that show very weak (within the noise level) to no fluorescence. (B-E) shows the normalized intensity of fluorescence of branch 1, cluster area, branch 2 and branch 3, respectively, as functions of time. The vertical axis is the dimensionless normalized intensity of fluorescence and the horizontal axis is the time in seconds in intervals of 1.2 s between recordings.

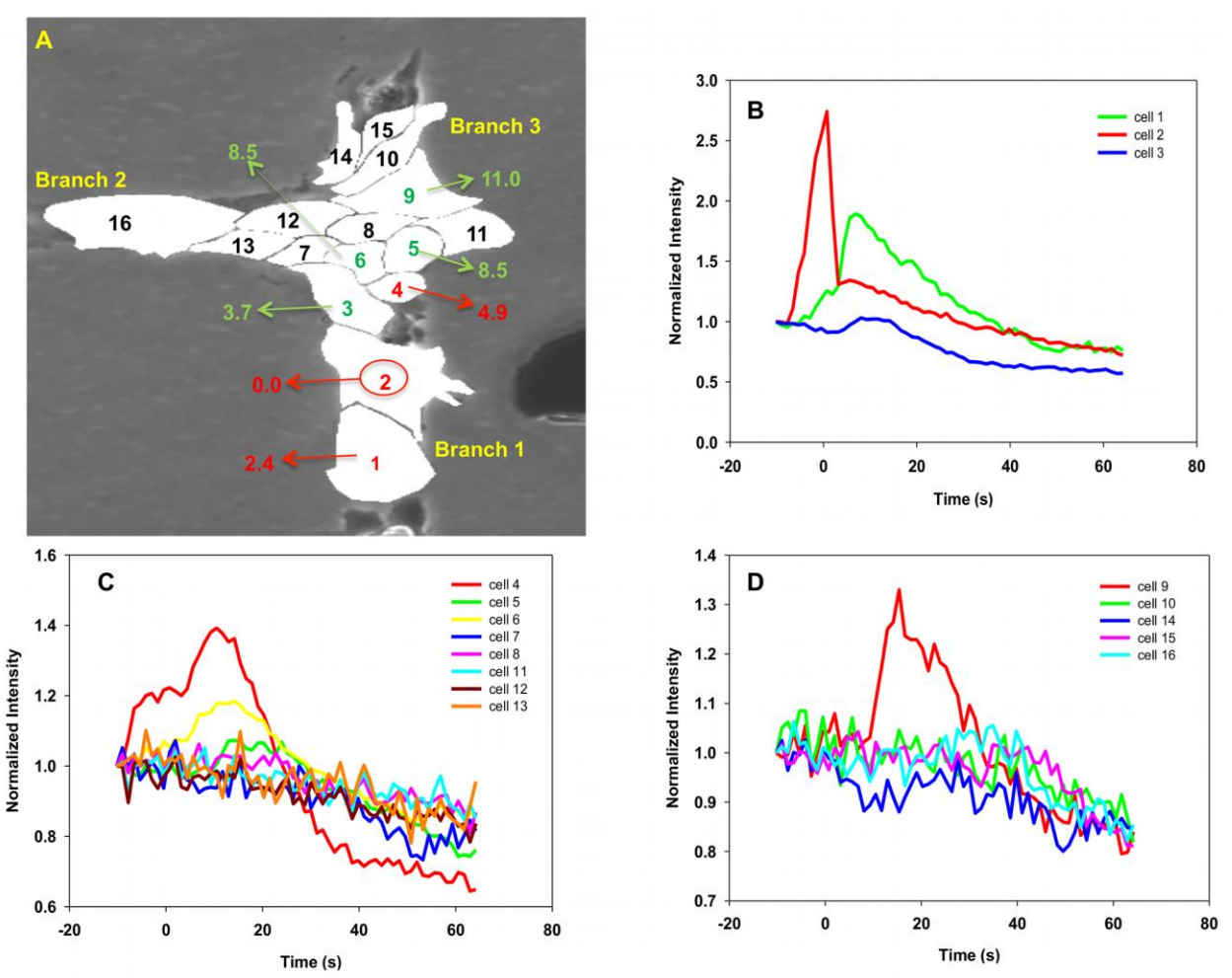

Figure 14. Experiment image 2 and normalized intensity of cells in "T" structure subjected to a single mechano-stimulation. (A) Image of a T structure of cells subjected to single mechano-stimulation. See Figure 13 for detail. (B-D) shows the normalized intensity of fluorescence of representative cells as functions of time. The vertical axis is the dimensionless normalized intensity of fluorescence and the horizontal axis is the time in seconds in intervals of 1.2 s between recordings.

In Figure **13**, two calcium signals originate from stimulated cell 4 (branch 1) and propagate into two directions, upward and downward. While the downward propagation is similar to that of a single chain although cell 1 (end cell of branch 1) does not respond, probably due to edge effects, and for our purposes, is not relevant. In contrast, a strong pulse propagates upward along a path involving cells 5 to 13. This pulse has similar characteristics as those observed in the non-branched single chains. The calcium-dependent fluorescence lessens in the

junction area and does not propagate beyond the junction area into the other two branches. From Figure **13**(D and E), there are two sudden peaks appearing in cell 21 and 26. However, these two peaks are likely individual firing events, which we have observed in several cases, because the neighboring cells do not exhibit significant response and/or the response time is not consistent with the average time of propagation from one cell to the next. A similar behavior occurs in the case of a truncated branch structure as shown in Figure **14**. The observed behavior may be understood on the basis of a competition between the intracellular dynamics of CICR and intercellular diffusion that depends on the architecture of the multicellular structure. Indeed, the fluorescence response of a cell results from the release of calcium by ER induced by a cytosolic calcium concentration that has risen above a threshold. This rise is due to an imbalance between inward and outward diffusion fluxes from and to neighboring cells. In a single chain, a cell that is being approached by a calcium wave has only two nearest neighbors and an excess of inward versus outward calcium diffusion will lead to rising cytosolic calcium concentration that will trigger CICR. If many inactivated cells surround a cell of interest such as in a cluster, these cells may serve as calcium sinks drawing calcium away from the cytoplasm of the cell of interest via diffusion. The calcium level in that cell may never reach the threshold needed to induce CICR. In a "T" structure, a calcium pulse propagating along a branch composed of a single chain of cells reaches the junction region composed of a cluster of cells. In this case, the calcium diffusion process transforms from diffusion in a one-dimensional space to diffusion in a two-dimensional space. The larger number of paths for diffusion between cells in the two dimensional region may prevent sufficient accumulation of calcium in any cell to trigger calcium release by ER. At the interface between the one-dimensional and two-dimensional regions and inside the junction cluster, for each cell outward diffusion exceeds inward diffusion and the calcium wave is

stopped. These experimental observations provide evidence for an effect of the architecture of multicellular structures on the propagation of calcium waves. We conducted 20 experiments similar to those reported in Figure **13** and Figure **14**, and half of them (10/20) showed that the calcium signal could transmit to more than one arm. However, upon detailed characterization of the multicellular structures, it appeared that many of the structures that showed transmission of the calcium signal beyond the junction-cluster region possessed structural imperfections such as stimulated branches that were two-cell wide. It is anticipated that calcium signal propagation from a two-cell wide branch to the junction region could not be considered as transitioning from a one-dimensional to a two-dimensional regions anymore. This will be the focus of a future study.

"T" Structure-Single Stimulation: Simulation

To shed light on the experimentally observed behavior of section "2.3.3-T Structure-Single Stimulus: Experimental" we develop a simplified model that mimics the structural characteristics of the experimental "T" network and can capture the effect of multicellular architecture on the competition between intracellular dynamics and intercellular diffusion. The model architecture is illustrated in Figure **15**(A). The structure is composed of a backbone chain containing 61 cells. Cells 30, 31 and 32 are junction cells. A side branch is connected to cell 31 and forms a right angle with the backbone. The side branch contains 30 cells denoted 1s, 2s, etc. Two additional cells 1' and 2' are located at the junction of the backbone and the side branch to mimic a cell cluster and multiple junctions. In the model, cells are represented as squares and we differentiate calcium diffusion between cells that are connected by their edges or by their vertices. The diffusion coefficient for edge-to-edge diffusion is the same as that used in modeling a single chain, namely D^*. Diffusion through vertices in the junction area, such as for instance between "cell 1s" in the side branch and cells 30 and 32 in the backbone, is characterized by a

dimensionless diffusion coefficient denoted $D^{*\prime}$. $D^{*\prime}$ is chosen to be smaller than D^{*} as the diffusion distance along a diagonal direction is larger than the cell-to-cell distance in a chain. Moreover, one also expects the density of gap junctions in a vertex-to-vertex contact area to be lower than in an edge-to-edge area.

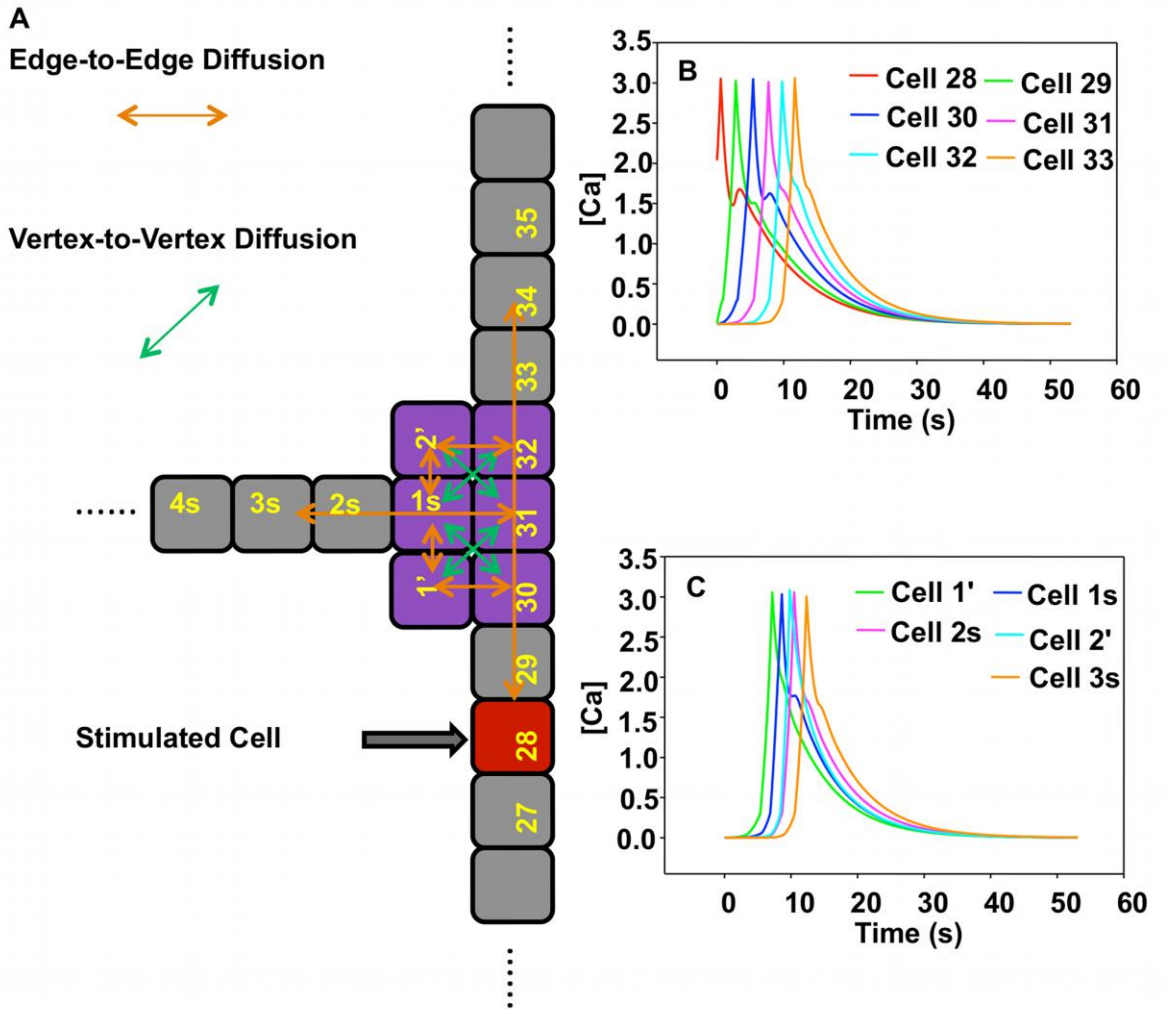

Figure 15. Schematic illustration and simulation results of the model "T" structure subjected to single stimulus. (A) Schematic illustration of the model "T" structure subjected to a single stimulus. Red cell is the stimulated cell. Orange arrows represent the edge-to-edge diffusion. Green arrows represent vertex-to-vertex diffusion. Purple cells highlight the junction cell cluster. (B) Calcium concentration of cells in backbone as a function of time. (C) Calcium concentration of cells 1', 2' and cells in the side branch. Here $\mathbf{D}^{*\prime} = \mathbf{0}$.

The reaction-diffusion equations for cells in the junction area are detailed in the Appendix I. We initially investigate the effect of the value of $D^{*\prime}$ on the behavior of the model system. When $D^{*\prime}$ ranges from 0.0 to 0.16, a calcium wave triggered at cell 28 propagates throughout the entire model structure including backbone, side branch and junction cluster (see Figure **15**(B) and (C)). For values of $D^{*\prime}$ in the range 0.17 to $D^{*} = 0.6$, the calcium wave originating at the stimulated cell is unable to propagate beyond the junction region (see Figure **16**).

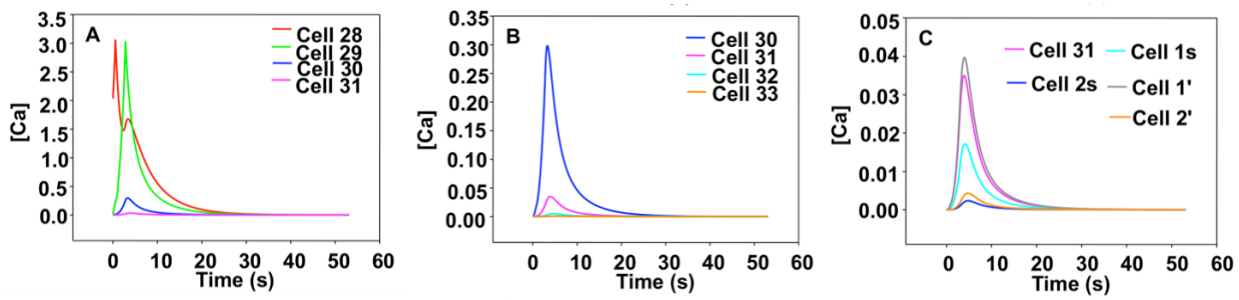

Figure 16. Simulated calcium concentration for cells in the "T" structure subjected to single stimulation with $D^{*\prime} = 0.2$. (A) reports the response of cells 28 to 31 in backbone as a function of time. (B) shows the calcium concentration of cells 30 to 33 in backbone as a function of time. Notice the change of scale of the vertical axis. (C) illustrates the calcium concentration of cells 31, 1' and 2' in the junction area and the side branch as a function of time. Again notice the change of scale of the concentration axis.

Cells in the junction area and the side branch exhibit very low levels of calcium. Figure **16** indicates for instance that due to the effect of vertex-to-vertex diffusion, the calcium concentration in cell 30 decreases too fast and cannot exceed the threshold UC_1 for inducing CICR. Subsequently, the calcium concentration decreases steadily in the junction area. With a larger $D^{*\prime}$ the junction region realizes a conversion from one-dimension-like diffusion to two-dimensional diffusion. The simulated behavior is comparable to that observed experimentally. This suggests that a calcium pulse cannot propagate in a multicellular structure with regions that transition from one-dimensional diffusion (in the lower branch of backbone) to two-dimensional

diffusion (in the junction cell cluster). These computational results provide further evidence for an effect of the architecture of multicellular structures on the propagation of calcium waves.

2.3.4 Double stimulation of "T" structure

In section "2.3.2-Single Chain-Dual Stimulation: Experiments" we have demonstrated that two calcium waves cannot cross when propagating toward each other in a chain of endothelial cells. We consider, here, the dual-stimulation of a "T" structure with stimulations located in two separate branches. We address the question of the interaction of the two calcium pulses in the junction area.

"T" Structure-Dual Stimulation: Experimental

To facilitate comparison between dual and single stimulation, two separate mechano-stimulations are applied on cells close to the junction in order to ensure that calcium waves would propagate well beyond the junction and into the side branches. Two calcium signals were generated from each stimulated cell. They propagate in two opposite directions. For instance, the calcium signal induced in cell 19 propagates upward toward the junction and downward along the chain of cells that constitute branch 1. Two of the pulses, generated from cell 2 and cell 19 respectively, meet in the junction area. The other pulse terminates at the ends of branches 1 and 3 (see Figure **17**).

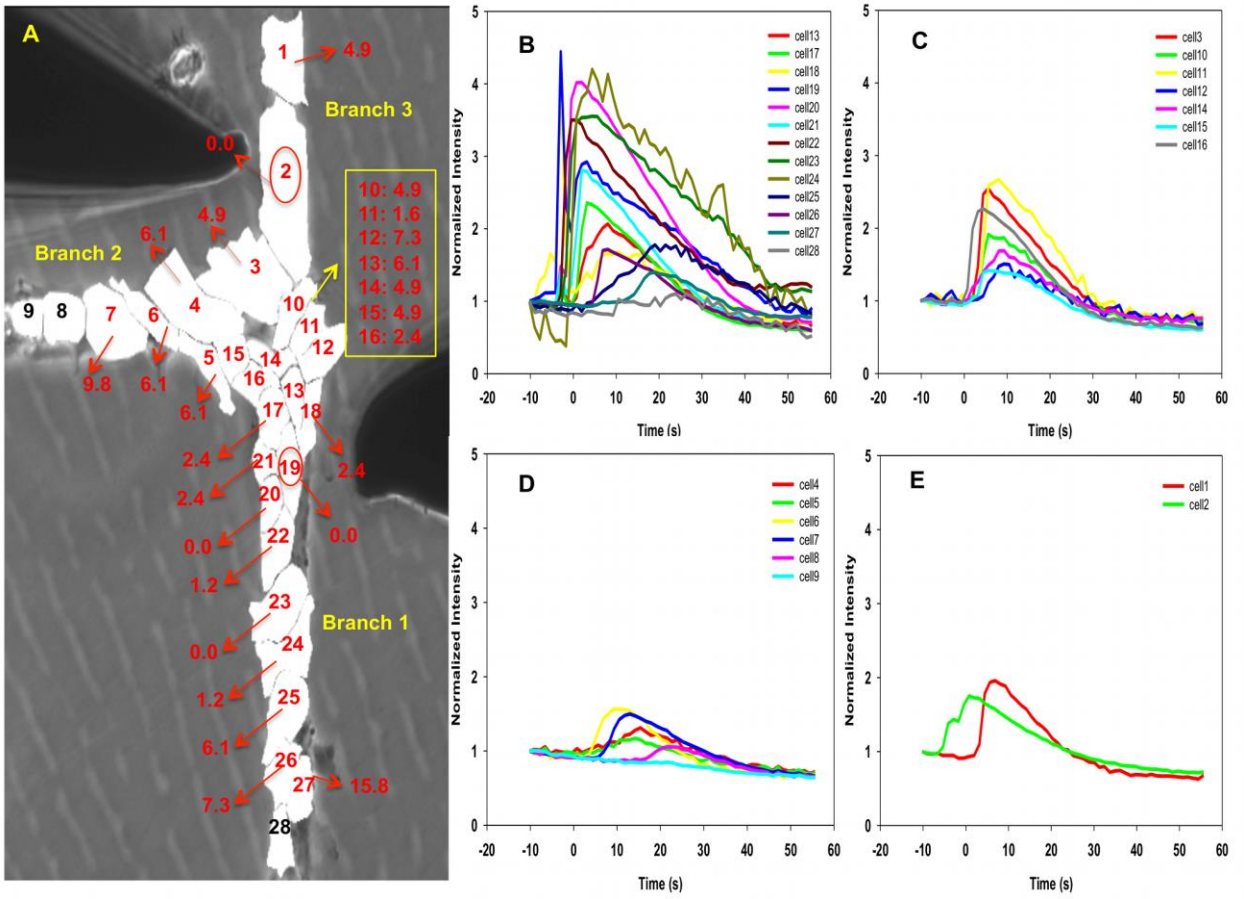

Figure 17. Experiment image and normalized intensity of cells in "T" structure subjected to double stimulation. (A) Image of a T structure of cells subjected to double mechano-stimulation. The red circle identifies the stimulated cells. Red labels indicate the response time individual cells. All the cells exhibited strong fluorescence with response times calculated from the rate of change of the fluorescence intensity. Black labels show cells exhibiting only noise level fluorescence. (B-E) show the normalized intensity of fluorescence of branch 1, cluster area, branch 2 and branch 3, respectively, as functions of time. The vertical axis is the dimensionless normalized intensity of fluorescence and the horizontal axis is the time in seconds in intervals of 1.2 s between recordings.

Figure **17** unambiguously shows that nearly every single cell in the "T" structure can support a calcium wave when it is subjected to a dual stimulation. The fluorescence intensity of every cell is strong and possesses the characteristics of pulses observed in the case of the single stimulation of single chains. In contrast to Figure **13** and Figure **14**, the cluster area in the junction is not acting as a diffusion sink for the calcium signal and the calcium wave is able to propagate

throughout the junction and beyond into branch 2. The signal terminates at cell 8 in branch 2 probably because it has reached its maximum travel distance or due to edge effects. Compared to section "2.3.3-T Structure-Single Stimulus: Experimental", the dual stimulation launches two calcium pulses toward the junction area. The initial time evolution of the calcium concentration in cells in the junction cluster is now driven by diffusion from several CICR activated cells. The activated cells surrounding a cell of interest in the cluster may serve as calcium sources providing calcium to the cytoplasm of the cell of interest via diffusion. This enables a rise in calcium concentration that can exceed the threshold for triggering subsequent CICR. This rise is now due to an imbalance between outward and inward diffusion fluxes from and to neighboring cells. The two sources of calcium can compensate for the transition from diffusion in the one-dimensional space of the stimulated branches to diffusion in the two-dimensional space of the junction area. We conducted 8 similar experiments and 6 out of 8 (0.75%) showed the same type of behavior.

"T" Structure-Dual Stimulation: Simulation

Figure **18** illustrates the response of the model "T" structure to two stimuli. The model system is identical to that introduced in section "2.3.3-T Structure-Single Stimulus: Simulation". All cells are initialized to a calcium concentration of 0 but cells 28 and 34, which are given simultaneously an initial concentration of C_0.

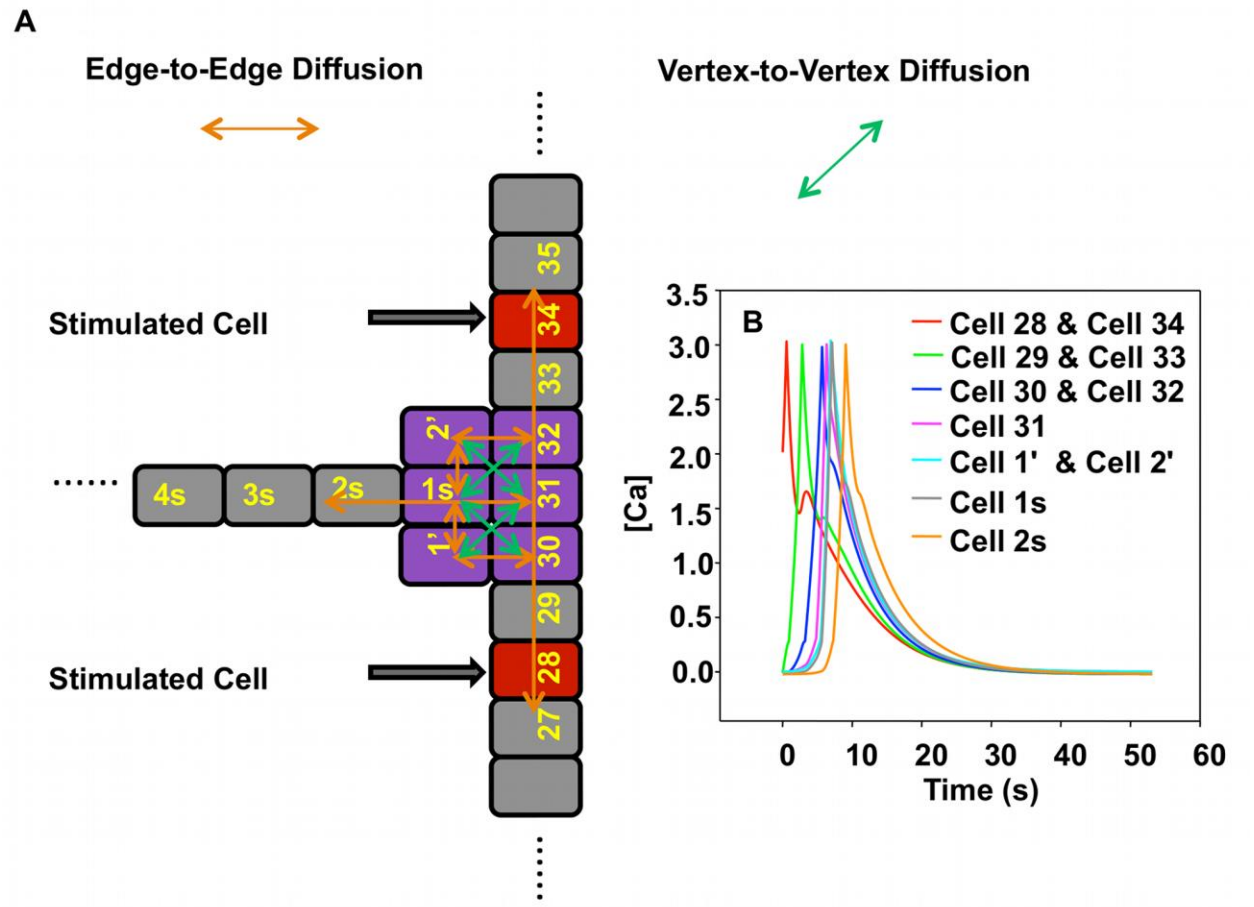

Figure 18. Schematic illustration and simulation results of the model "T" structure subjected to double stimulus. (A) Schematic representation of "T" structure of cells subjected to dual stimulation. Red cells are the stimulated cells. See Figure 15 for additional details. (B) Calcium concentration as a function of time for cells in the vicinity of the junction. $\mathbf{D^{*\prime} = 0.2}$.

We consider the case of $D^{*\prime} = 0.2$ for which we have previously shown the inability to support a propagating calcium wave when it is induced by a single stimulation. Figure **18**(B) shows that a calcium wave propagates readily throughout the junction area and into the side branch. Further investigation of the effect of the vertex-to-vertex diffusion coefficient shows that the calcium wave propagation is limited to values of $D^{*\prime}$ in the range of 0.00 to 0.23. Beyond the value of 0.23, $D^{*\prime}$ does not allow the "T" structure to support propagation into the side branch as fast diffusion in the cluster would prevent cytosolic calcium concentrations to exceed the CICR threshold. Therefore, in light of the simulations of the "T" structure subjected to single and dual

stimulation, agreement with the experimental observations is achieved when $D^{*\prime} \in [0.17,0.23]$. As in the simulations and cell chain experiments, calcium signals propagate through a "T"-like structure of arterioles in the intact microvasculature, a more native architecture, when stimulated chemically by applying acetylcholine as agonist. While our emphasis has been on endothelial cells, this type of behavior likely depends on cell-type, morphology, the nature of the stimulation and environment [52].

2.4 Summary

In this chapter, we study experimentally the propagation of calcium waves in different multicellular structures composed of human umbilical vein endothelial cells (HUVEC). The fabrication of cell-chain based multicellular chain structures relies on organizing multiple cells into specific configurations via selective plasma surface functionalization, which guides cellular attachment. Calcium waves are actuated via mechano-stimulation of selected cells. Calcium wave propagation is characterized by time-resolved fluorescence microscopy. The experimental observations are complemented by modeling and simulation of calcium wave propagation using a diffusion/reaction model. The model of intracellular calcium dynamics is non-linear and mimics the IP_3-induced calcium release and calcium induced calcium release (CICR). In order to capture the essence of cross-level interactions in calcium signal propagation in multicellular architectures, we only consider a single component model of CICR. This model is different from previous CICR models, which consisted of multiple coupled non-linear differential equations describing the kinetics of IP_3/Ca^{2+} pumping, release and activation [18,54]. Nevertheless, the model is capable of capturing most essential features of calcium wave propagation in HUVEC observed in the experiment.

Cell-to-cell interactions are described in this paper via intercellular diffusion through gap junctions. Experimental observation of calcium waves induced by a single mechano-stimulation and propagating along a chain of endothelial cells is used to calibrate the model. Experiments and simulations of chains of cells subjected to dual stimulation (i.e. simultaneous stimulation of two different cells) show that two calcium waves cannot cross each other due to the refractory stage of endothelial cells. The study of more complex multicellular structures utilized "T" structures, which are composed of three side branches joining at a junction. The junction is comprised of cell clusters. In this case, we observe experimentally that when a single cell in one of the side braches is stimulated, the calcium signal does not propagate beyond the junction area. However, when two mechano-stimulations are simultaneously applied on separate branches the calcium signal can propagate through the junction area and beyond well into the third unstimulated side branch of the "T" structure. A computational model of a "T" structure, which includes a cell cluster at the junction, shows the importance of intracellular calcium dynamics and intercellular diffusion in determining the propagation behavior of calcium waves. In particular, the organization of cells in the junction determines the existence of multiple paths for intercellular diffusion, which may affect the accumulation of cytosolic calcium and subsequently the ability of cells to undergo CICR.

In summary, this work demonstrates that the propagation of calcium waves is dependent upon the architecture of multicellular structures. This dependence is due to the competition between intracellular calcium reaction and diffusion, which is affected by the topology through cell connectivity via gap junctions.

CHAPTER 3. REGULATION OF THE FREQUENCY AND WAVELENGTH OF CALCIUM WAVES PROPAGATING IN NETWORKS OF INTERCONNECTED CELLS: A SIMULATION STUDY

In the previous chapter, we introduce a combined theoretical and experimental study of the propagation of calcium signals in multicellular structures subjected to mechano-stimuli. However, in many cell types, extracellular chemical stimuli can be converted into intracellular signal in forms of $[Ca^{2+}]_c$ oscillation [55]. This intracellular calcium oscillation accounts for the chemical reaction and diffusion of cytoplasmic calcium and inositol-1,4,5-triphosphate (IP_3). Its frequency strongly depends on the dose of the applied extracellular agonist, whereas, the oscillation amplitude is nearly constant [56]. In this chapter, I will introduce a more complicated model of calcium wave propagation in a chain of cells incorporating both intracellular calcium dynamics and intercellular calcium wave propagation. We investigate computationally the effect of cross-level interdependence between intracellular calcium-IP_3 pathway and cell-cell communication via intercellular diffusion of both Ca^{2+} and IP_3. In contrast to Goldberg's model [57], diffusion in our model is linear with a diffusion coefficient that is independent of Ca^{2+}/IP_3 concentration. However, to achieve long-distance intercellular calcium wave propagation, a regeneration mechanism of IP_3 is evoked. This mechanism depends on the cytosolic Ca^{2+} concentration. We investigate the effect of the chain-like architecture of the multicellular network on the frequency of calcium oscillations of individual cells and the wavelength of trains of calcium waves. Significant cross-level effects are found on the transient behavior of individual cells as well as their steady oscillatory state.

3.1 Introduction

A particularly relevant aspect of networks, including cellular networks, is the potential emerging behavior of the system beyond simply a summation of individual element activities. With respect to cellular networks, the passing of signals between cells of the network is one way in which new system behaviors can emerge. For instance, intercellular calcium waves were observed to define communication networks among neural progenitor cells [58]. Also astrocytes of the cortical gray matter appear to play an active role in brain function that takes the form of calcium waves that propagate between cells within networks of astrocytes [59]. Central to understanding these emergent processes is that cellular networks inherently combine dynamical and structural complexity, making it difficult to isolate single cell versus emergent network behavior. However, the relationships between network dynamics and architecture have been successfully investigated using a variety of physical and mathematical approaches [38], many of which have been applied to understand the complexities of neuronal circuitry. For example, embryonic stem cell-derived neural progenitors form networks exhibiting synchronous calcium signaling activity. This coherent calcium dynamic was shown to be correlated across so-called small-world networks [60]; networks with the mean shortest distance between nodes scaled logarithmically with the number of nodes.

The objective of the present study is to develop a model-based theoretical framework to shed light on the phenomenon of cross-level interactions in complex and dynamic multicellular structures with a focus on calcium signaling via calcium waves. Calcium signaling occurs in nearly all cell types and calcium waves are a common phenomenon in multicellular systems. In particular, we are interested in the interplay between intracellular calcium activity and intercellular propagation in networks of cells. From a theoretical perspective, Othmer and

Scriven [61] developed, following Turing's pioneering mathematical treatise of morphogenesis [62], an analysis technique in which the information about the underlying network topology, through a connectivity matrix, is decoupled from that of the intracellular reaction pathway mechanism, thus enabling progress in multicellular network research that includes complexity at both low and high levels. A previous series of studies [39,40] reported the use of the Green's function-based Interface Response Theory (IRT) [63], a method originally developed for tackling composite media in condensed matter physics, to augment Scriven-Othmer's method to solve coupled dynamical networks with nontrivial connectivity matrices and therefore integrate natural biological organization from the cellular level to complex network architectures. We also conducted an experimental and computational study of calcium wave propagation in chains of model cells with nonlinear intracellular calcium dynamics and shown the importance of local cell environment on the transmission of a pulse through junctions in multicellular networks [64] (see chapter 2 for detail).

In this chapter, we show that the intracellular oscillation frequency of an individual cell embedded in the chain-like network and stimulated with an agonist differs at steady state from that of an isolated cell. Furthermore, the transient behavior of that stimulated cell toward steady oscillations is taking significantly longer in the multicellular network. In fact, the stimulated cell generates sequential trains of pulses with increasing frequency. These trains of pulses are supported and propagating along the chain of cells. The mechanism for this long time transient behavior is attributed to retrograde diffusion of calcium and IP_3 originating from a widening range of cells in the chain undergoing oscillations as the trains of pulses propagate. This mechanism highlights the importance of microenvironment on the dynamical behavior of cells in multicellular networks. In particular, this study demonstrates that the dynamical behavior of a

specific cell embedded in a multicellular environment depends on crosstalk between the cell and its environment.

3.2 Models and Methods

3.2.1 Model of intracellular calcium pathway

A schematic of our model for the dynamics of intracellular calcium oscillations and intercellular calcium diffusion is shown in Figure **19**. The pathway involves primarily the intracellular reaction dynamics and the intercellular diffusion of cytoplasmic calcium and inositol-1,4,5-trisphosphate (IP_3). The intracellular chemical reaction process is based on a model introduced by Politi *et al.* [65]. For the sake of clarity, we describe this model in some details. The intracellular calcium pathway starts with an extracellular agonist combines with the G-protein-coupled receptors on the cell's membrane to activate phospholipase C (PLC). It is, in turns, able to catalyze the production of IP_3 [66]. IP_3 then can bind to the IP_3 receptor, IP_3R, to open calcium channels in the membrane of the Endoplasmic Reticulum (ER). This process releases stored Ca^{2+} into the cytosol. Meanwhile, the cytoplasmic Ca^{2+} creates both positive and negative feedback conditions in the production of IP_3. For the positive feedback condition, the cytoplasmic Ca^{2+} is capable of activating the PLC isoforms to release more IP_3 [67]. For the negative feedback condition, the increase of cytoplasmic Ca^{2+} can activate the IP_3 degradation via IP_3 3-kinase (IP_3K). Because high levels of intracellular calcium are toxic and cannot be degraded as many other signaling molecules can, cells control the intracellular calcium level by buffering, sequestering in specialized compartments, and expelling to the extracellular space [50, 68].

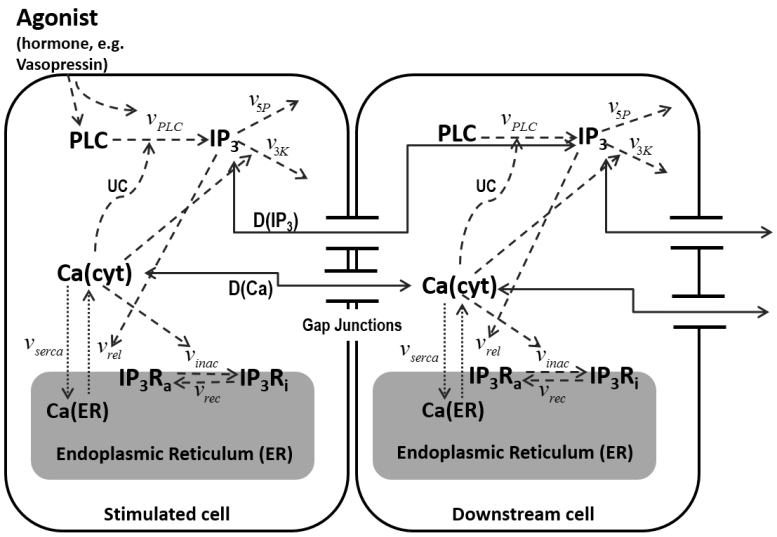

Figure 19. Reaction/Diffusion process of Ca^{2+} and IP_3 metabolism included in the model. The solid, dashed, and dotted arrows indicate molecular diffusion, regulatory interactions, and reaction/transport steps respectively. The bold quantities indicate the following model variables: IP_3, the cytoplasmic IP_3; Ca(*cyt*), the free cytoplasmic Ca^{2+}; Ca(*ER*), the free Ca^{2+} in the ER; IP_3R_a, the active conformation of the IP_3R. The other abbreviations denote IP_3R_i, the inactive conformation of the IP_3R; v_{serca}, the active Ca^{2+} transport into the ER; v_{PLC}, the production rate of IP_3; v_{rel}, the rate of Ca^{2+} release through the IP_3R; v_{inac} and v_{rec}, the rates of Ca^{2+}-induced IP_3R inactivation and recovery, respectively; v_{5P} and v_{3K}, the rates of IP_3 dephosphorylation and phosphorylation, respectively; D(*IP*$_3$) and D(*Ca*), the diffusion coefficient of IP_3 and Ca, respectively; and UC, the threshold of Ca needed to activate PLC.

The intracellular chemical reaction dynamics is formulated into a system of coupled differential equations involving four dynamical variables: the calcium concentration in the cytosol, *c*; the IP_3 concentration in the cytosol, *p*; the calcium concentration in the ER stores, *s*; and the fraction of IP_3R that has not been made inactivate by Ca^{2+}, *r*. The rate equation for the IP_3 concentration takes the following form:

$$\frac{dp}{dt} = f(c,p) = v_{PLC} - v_{\deg} = v_{PLC} - (v_{5P} + v_{3K}) = \left(V_{PLC} \frac{c^2}{K_{PLC}^2 + c^2} \right) - \left(k_{5P} + k_{3K} \frac{c^2}{K_{3K}^2 + c^2} \right) p , \quad (3\text{-}1)$$

where the v_{PLC} and $v_{\deg}$ represent the production and degradation rate of IP_3, respectively. V_{PLC} is the maximum production rate of PLC that depends on the agonist concentration. K_{PLC} characterizes the sensitivity of PLC to Ca^{2+}; v_{3K} and v_{5P} are the rates of IP_3 phosphorylation and dephosphorylation, respectively. Noted that the phosphorylation rate k_{3k} is described by a Hill function with the half-saturation constant K_{3K} [69]. The rate equation for the cytoplasmic Ca^{2+} is in the following form:

$$\frac{dc}{dt} = g(c,p) = v_{rel} - v_{serca} = \left[k_1 \left(r \frac{c}{K_a + c} \frac{p}{K_p + p} \right)^3 + k_2 \right](s - c) - V_{serca} \frac{c^2}{K_{serca}^2 + c^2}. \qquad (3\text{-}2)$$

For the sake of simplification, the total calcium concentration in the cell, c_{tot}, is conserved and is represented as $c_{tot} = c + \beta s$, where β is the ratio of effective cytoplasmic volume to effective ER volume (both accounting for Ca^{2+} buffering). Therefore, the calcium concentration in the ER store can be expressed as

$$s = \frac{c_{tot} - c}{\beta}. \qquad (3\text{-}3)$$

The dynamics of IP_3R inactivation by Ca^{2+} is shown as follow:

$$\frac{dr}{dt} = v_{rec} - v_{inac} = \frac{1}{\tau_r} \left(1 - r \frac{K_i + c}{K_i} \right). \qquad (3\text{-}4)$$

In our numerical simulations of the intracellular pathway, we use the model parameters reported by Politi [65]. We limit ourselves to the model supporting calcium positive feedback, in

which the phosphorylation rate k_{3k} is set to zero. The corresponding parameters are summarized in Table 4. The numerical solutions of these differential equations are obtained by using the 4th-order Runge-Kutta algorithm with step size, Δt =0.01 s.

Table 4. Values of reaction/diffusion model's parameters

Parameters	**Description**	**Value**
	IP_3 dynamics parameters	
K_{3K}	Half-activation constant of IP_3K	0.4 μM
k_{3K}	IP_3 phosphorylation rate constant	0
k_{5P}	IP_3 dephosphorylation rate constant	0.66 s^{-1}
K_{PLC}	Half-activation constant of PLC	0.2 μM
V_{PLC}	Maximum production rate of IP_3	1.5 μM s^{-1}
	Ca^{2+} transport and structural parameters	
β	Ratio of effective volumes ER/cytosol	0.185
V_{serca}	Maximal SERCA pump rate	0.9 μM s^{-1}
K_{serca}	Half-activation constant	0.1 μM
c_{tot}	Total Ca^{2+} concentration	2 μM

	IP_3R parameters	
k_1	Maximal rate of Ca^{2+} release	1.11 s^{-1}
k_2	Ca^{2+} leak	0.0203 s^{-1}
K_a	Ca^{2+} binding to activating site	0.08 μM
K_i	Ca^{2+} binding to inhibiting site	0.4 μM
K_p	IP_3 binding	0.13 μM
τ_r	Characteristic time IP_3R inactivation	12.5 s
	Reference Diffusion parameters	
D^*_{Ca}	Diffusion coefficient rate of Ca^{2+}	0.005 s^{-1}
D^*_{IP3}	Diffusion coefficient rate of IP_3	$10\,D^*_{Ca}$
UC	Threshold of Ca^{2+} to activate PLC	0.057 μM

We illustrate the oscillatory behavior of the intracellular calcium concentration of individual cell in Figure **20**. Following Politi, we can increase the frequency of the intracellular calcium oscillations by increasing the agonist concentration. For an isolated cell, the frequency of intracellular calcium oscillation does not vary so much at constant V_{PLC} (see Figure **20**). The IP_3 activity follows a similar dynamics.

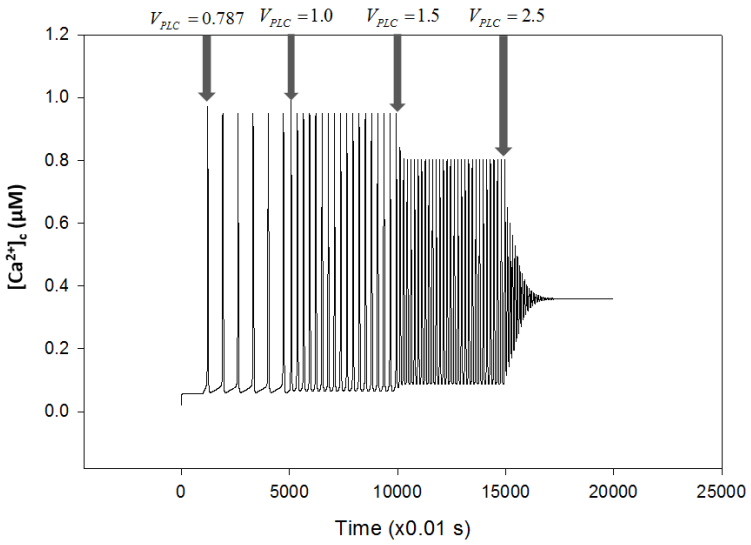

Figure 20. Politi model: Agonist-induced intracellular calcium oscillation with stepwise increases in the agonist concentration (arrows) corresponded by an increase in V_{PLC}. The Y-axis represents the cytosolic calcium concentration with unit "μM." The X-axis represents the time with unit "0.01 s." V_{PLC}=0.3 μM s^{-1} for t < 1000 with successive increases to 0.787, 1.0, 1.5, and 2.5 μM s^{-1}.

Figure **21** illustrates the period of intracellular calcium oscillation generated in an isolated cell with initial calcium concentration, $[Ca]_i$=0.05 μM. Initially, the period between the oscillating peak #1 and #2 is 1787 time steps. However, the period between the peak #2 and #3 sharply decreases to 1681 time steps (point #2 in Figure **21**), which is followed by a steady state with the period equal to 1672 or 1673 time steps. We have verified that different initial concentrations result in the very similar period behavior.

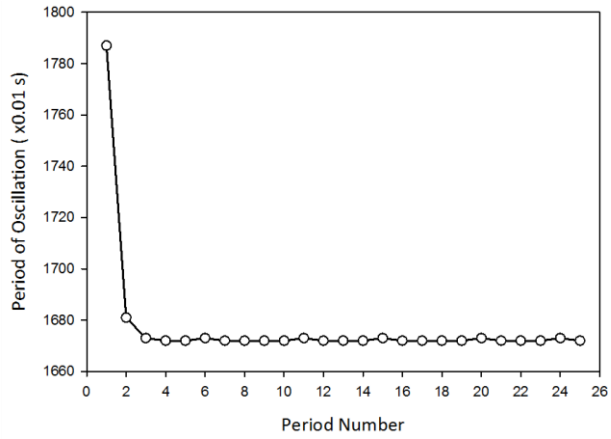

Figure 21. Period of intracellular calcium oscillation in an isolated cell. The X-axis represents the subsequent maxima. The Y-axis represents the value of time (in units of 0.01 s) corresponding to the occurrence of each maximum.

3.2.2 Integration of intracellular calcium pathway into multicellular diffusion model

Politi's model only considers the intracellular dynamics in an isolated cell. To use Politi's model to describe the calcium and IP_3 dynamics in a multicellular system, we need to add the phenomenon of diffusion of both Ca^{2+} and IP_3 driven by the concentration gradients between neighboring cells. The multicellular structure considered in this model is composed of a single linear chain of N cells with periodic boundary conditions (PBC). In such a chain, in which every cell is connected to two other cells (diffusion between nearest neighbor cells), one can write the one-dimensional time-dependent reaction/diffusion equation for Ca^{2+} and IP_3:

$$\frac{\partial c}{\partial t} = D_{Ca}\frac{\partial^2 c}{\partial x^2} + g(c,p) = D^*_{Ca}\left[c(x_{i+1},t_n) - 2c(x_i,t_n) + c(x_{i-1},t_n)\right] + g(c,p), \tag{3-5}$$

and

$$\frac{\partial p}{\partial t} = D_{IP3}\frac{\partial^2 p}{\partial x^2} + f(c,p) = D^*_{IP3}\left[p(x_{i+1},t_n) - 2p(x_i,t_n) + p(x_{i-1},t_n)\right] + f(c,p), \tag{3-6}$$

where "D_{Ca}" and "D_{IP3}" are the diffusion coefficients of Ca^{2+} and IP_3. "*x*" and "*t*" are the position and time variables. In Eq. (3-5) and (3-6), we have discretized the equation in space and time using finite differences. "$t_n = n\Delta t$" refers to the discretized time line with a time step of Δt. $D_{Ca}/\Delta x^2$ and $D_{IP3}/\Delta x^2$ are defined as the diffusion coefficient rate of Ca^{2+} and IP_3 with unit "per second", "s^{-1}", which we denote D^*_{Ca} and D^*_{IP3}, respectively. "Δx"refer to the nearest neighbor intercell-distance. To implement PBC, we impose the cyclic condition on the index "*i*": cell *i*+1=*cell* 1 if *i*=N and cell *i*-1=*cell* N if *i*=1. The term on the left-hand side is the rates of change of intracellular Ca^{2+}/IP_3 concentration in cell "*i*". The concentration for the next time increment, *n*+1, can be calculated from concentration values at the previous time increment, *n*. We assume that diffusion occurs only between nearest neighboring cells through their membrane via gap junctions. We further assume that the distribution of gap junctions in the plasma membrane is spatially uniform and that the diffusion coefficients are constants independent of cell number. Note that the mobility of Ca^{2+} through gap junction is restricted in comparison to that of IP_3 because of the higher buffering capacity of cytoplasm for Ca^{2+} than for IP_3 [24]. Thus, IP_3 diffuses much faster than Ca^{2+} [53]. For the sake of simplicity, we set $D^*_{IP3} = 10D^*_{Ca}$ in our model.

In combining intracellular dynamics and intercellular diffusion, at a given time, t_{n-1}, for each cell "*i*", we effectively solve Eq. (3-1), (3-2) and (3-4) by using the 4th order Runge-Kutta method to evolve the *c* and *p* concentrations at the time, t_n, due to intracellular dynamics. Meanwhile, the updated $p(x_i, t_n)$ and $c(x_i, t_n)$ are used in the diffusion part of Eq. (3-5) and (3-6) to impact the Ca^{2+}/IP_3 concentration in the neighboring cells. We have verified that this algorithm has fully converged for the time step Δt =0.01 s. For this we have implemented the

algorithm for smaller time steps of $\Delta t/2$ and $\Delta t/4$ verified that one obtains the same reaction/diffusion dynamics.

To study the propagation of trains of calcium waves in a multicellular one-dimensional chain, we initially stimulate a single cell in the center of the chain with the agonist. This cell will be called subsequently: "stimulated cell." PLC of the stimulated cell is activated initially by the extracellular agonist to induce intracellular Ca^{2+}/IP_3 oscillations. All other cells in the chain that are not initially stimulated ($V_{PLC} = 0$) are referred to as "downstream cells." One may visualize the downstream cells as forming a cellular microenvironment in which the stimulated cell is embedded.

The reaction dynamics of the stimulated cell increases its calcium concentration. Diffusion of Ca^{2+} between the stimulated cell and its neighboring downstream cells elevates the Ca^{2+} concentration in downstream cells. To enable the propagation of a train of calcium waves that is initiated by the oscillation of the stimulated cell, we introduce a threshold based on the calcium concentration for inducing Ca^{2+}/IP_3 positive feedback in downstream cells (Figure **19**). When the cytoplasmic Ca^{2+} concentration reaches a value exceeding a threshold, *UC*, the positive feedback effect of cytoplasmic Ca^{2+} is activated to increase the production rate of IP_3. If the cytoplasmic Ca^{2+} concentration is below the threshold, PLC isoforms are not activated. This enables the synchronized development of collective spatio-temporal response of multicellular architectures. This extension is based not only on diffusion but also on an additional amplification mechanism through the generation of IP_3 and the Ca^{2+}-dependent activation of PLC [70].

In the simulation, the multicellular chain consists of 301 cells. The central cell (cell 151) is the stimulated cell. The size of the chain is chosen such that the calcium trains of waves never reach the ends of the chain (cells 1 and 301) during the time of the simulation. So even though we have implemented PBC, these conditions are never required during the simulation time reported here. The initial concentrations of Ca^{2+} and IP_3 are set to 0.05 μM. The continuous presence of agonist is required to evoke the sustained intercellular calcium waves [71]. Therefore, the V_{PLC} of the stimulated cell is kept at 1.5 μM s^{-1}. All other cells have their initial V_{PLC} set to zero. When the calcium concentration exceeds UC for the first time in a downstream cell, its V_{PLC} is set to 1.5 μM s^{-1} for the remaining time of the simulation. The parameters of the diffusion model are listed in Table 4 with those parameterizing the intracellular reaction dynamics.

3.3 Results and Discussion

A comparison between the calcium oscillation of the stimulated cell and its first neighboring downstream cell is shown in Figure **22**. Because the diffusion process is symmetric, we just show the temporal evolution of the calcium concentration on one side of the chain. The IP_3 activity shows a similar dynamic.

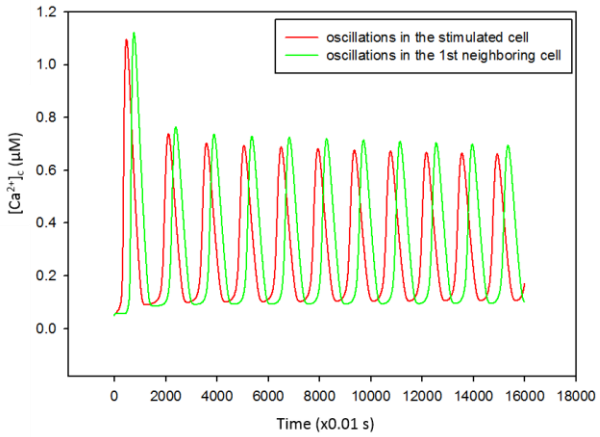

Figure 22. Calcium oscillation based on reference parameters in stimulated cell and its first neighboring cell. The Y-axis represents the cytosolic calcium concentration with unit "μM." The X-axis represents the time unit "0.01 s." The red line stands for the intracellular calcium oscillation in the stimulated cell. The green line shows the intracellular calcium oscillation in the 1st neighboring cell.

Initially, only the stimulated cell is triggered to generate calcium oscillation. Meanwhile, cytosolic calcium diffuses from the stimulated cell to the downstream cells through gap junctions. Once the calcium concentration in the downstream cells rises to a level exceeding the threshold "*UC*," the PLC in the downstream cells is activated, that is, we set $V_{PLC}^{dc} = V_{PLC}^{sc} = 1.5$ μM s^{-1}, where the superscripts "sc" and "dc" denote "stimulated cell" and "downstream cells", respectively. This process sustains the propagation of a calcium wave. In Figure **22**, the cytosolic calcium oscillation frequency of both the stimulated cell and the 1st neighboring cell is nearly the same. However, a slight phase shift occurs in the 1st neighboring cell because of a time lag imposed by the Ca^{2+}/IP_3 diffusion process. This latency is inversely proportional to the value of the diffusion coefficients. The IP_3 activity shows similar dynamics.

We now turn to a full description of the propagation of calcium train of waves resulting from the coupled reaction/diffusion model (see Figure **23**).

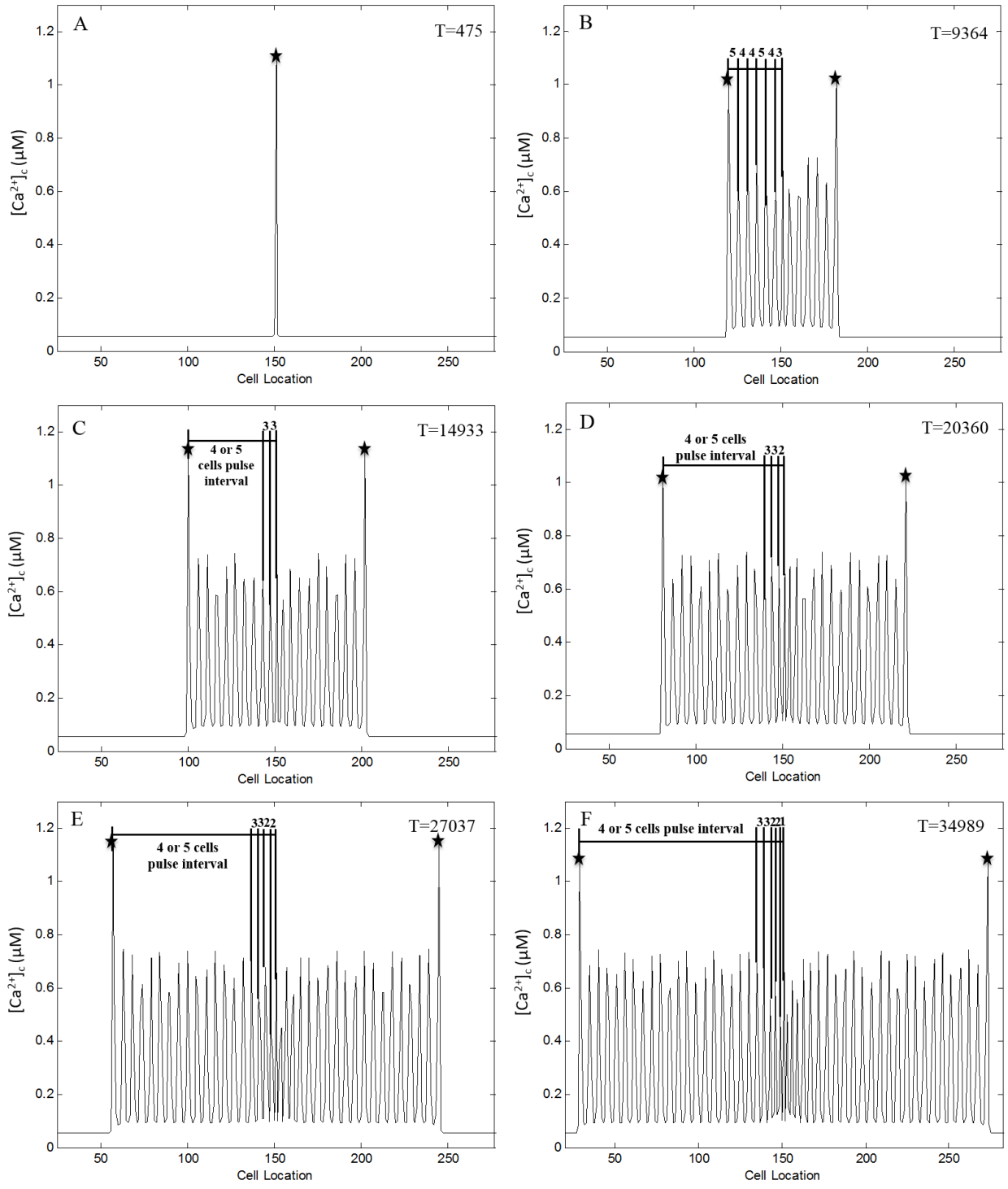

Figure 23. Snapshots of the propagating train of waves along the chain of cells. The snapshots are reported at different times expressed in units of "0.01 s." The Y-axis represents the cytosolic calcium concentration. The X-axis represents the location of cells. Cell 151 is the stimulated cell. (A) Train of pulses at time point T=475; the front of the train of pulse is marked by a star, "★,"and this in subsequent snapshots. (B) Train of pulses at time point T=9364; the separation distance between pulses

(wavelength of the train) amounts to a segment of the chain containing 4 to 5 cells for the first 6 pulses. This wavelength reduces to a segment containing 3 cells between pulse # 7 and # 6. (C) Train of pulses at time point T=14933; the train of pulses keeps propagating and retains a wavelength of 4 to 5 cell segments between pulses #1 through #9. The wavelength amount to a 3 cell segment between pulses #9 and #11. (D) Train of pulses at time point T=20360; the central area with short wavelength expands spatially; the pulse interval between the newest calcium pulse generated by the central cell and the adjacent pulse decreases to a 2-cell segment. (E) Train of pulses at time point T=27037; the central region with decreasing wavelength keeps expanding. (F) Train of pulses at time point T=34989; short wavelength region expands further and the wavelength shortens to 1-cell interval.

Figure **23** illustrates the temporal and spatial evolution of the train of calcium waves produced by the multicellular reaction/diffusion model. Initially, intracellular calcium oscillation is induced by the extracellular agonist in the central cell (cell 151). At the time step T=475 (in units of 0.01s), the first calcium pulse in the central cell, which is marked by a star, "★," reaches its highest value (Figure **23** *A*). As time marches, this pulse splits into two pulses, propagating in opposite directions from the stimulated cell. Because pulse propagation is symmetrical about the center of the chain, we number the pulses from the pulse at the front of the train on the left side of the stimulated cell, only. The pulse labeled with a "star" corresponds to the 1st pulse, or say pulse #1 in the train. As time proceeds, the central cell undergoes subsequent oscillations. These oscillations emit calcium pulses that propagate in opposite directions along the chain. This process leads to the formation of the two opposite intercellular calcium wave trains (ICWTs). The wavelength of the ICWTs (separation distance between adjacent pulses) will be quantified by the number of cells between two maxima. It takes a value between 4 and 5 cells. After the 7th oscillation of the stimulated cell, at T=9364, pulse #1 is located on cell 120. The 7th calcium pulse supported by the central cell reaches its highest level when the 6th pulse reaches cell 147 (Figure **23** *B*). The interval between these two pulses now corresponds to a segment containing 3 cells (involving cells 148, 149, 150). This is the beginning of the a spontaneous heterogenization

of the train of pulses propagating along the chain of cells, that is a time-dependent decrease in the wavelength of the train of pulses At T=14933, when the calcium concentration in the central cell reaches its 11^{th} maximum, the train of pulses is composed of two distinct regions. A train of pulses with a 4- to 5-cell wavelength (between pulses 1 and 9) and a central regions with three pulses (#9 to #11) separated by segments containing 3 cells (Figure **23** *C*). At T=20360, the central region of the chain becomes even more heterogeneous as a wavelength of 2-cell interval appears between pulses #15 and #14 (Figure **23** *D*) in addition to the existing 3-cell interval wavelengths already described. For T=27037, the central region is composed of five pulses with 2-cell and 3-cell wavelengths (Figure **23** *E*). Finally, the train of pulse is fully heterogenized with 4- to 5-cell distances separating the pulses #1 to #21, and a central region composed of pulses #21 through #26 separated by 3-, 2- and 1-cell wavelength. The wavelength of the train of waves decreases as one approaches the stimulated cell from the front pulse (Figure **23** *F*). Although we only reported calcium concentration in Figure **23**, the concentration of IP_3 follows a very similar dynamics.

Figure **24** illustrates the downward tendency of the period of intracellular calcium oscillation generated in the stimulated cell. Similar to Figure **21**, the period of oscillation shown in Figure **24** begins with a sharp decrease followed by a slow reduction before reaching a constant value. The initial rapid decrease is similar to that observed for the isolated cell in Figure **21**. This is representative of the dynamics of the intracellular pathway. However, the slow varying region of Figure **24** contains 21 points (point #2 to #22, i.e. 21 periods) instead of 2 points (point #2 and #3) as was shown in Figure **21**. Moreover, the period of oscillation at steady state in Figure **24** is smaller than that in Figure **21**. We observe two effects, these being: (a) a slow rate of evolution toward steady state in the multicellular structure compared to the isolated cell, and (b) a steady

state period of oscillation that depends on the cell environments indicate that the intracellular dynamics is probably controlled by the diffusion process.

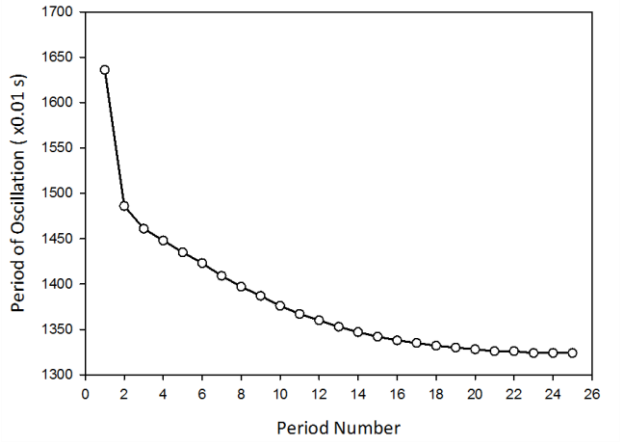

Figure 24. Period of intracellular calcium oscillation in the central cell. The X-axis represents the subsequent maxima. The Y-axis represents the value of time (in units of 0.01 s) corresponding to the occurrence of each maximum.

The calcium diffusion process is bi-directional and is driven by the calcium concentration gradient between the neighboring cells. We name the diffusion from the center of the chain to the edges of the chain the "forward diffusion" and the diffusion from the edges to the center the "retrograde diffusion." When the calcium pulses in the central cell split into two pulses that subsequently propagate outward, the calcium concentration of the central cell decreases to form a trough while the calcium concentration of the downstream cells remains high. Thus, a calcium concentration gradient is established between some of the downstream cells with high calcium concentration and the cells in the vicinity of the central cell with low calcium concentration. Retrograde diffusion will occur, increasing slightly the Ca^{2+} concentration in the central region of the chain. The central cell may, therefore, take less time to reach its highest calcium level. With an increase in the number of calcium pulses along the cell chain, the influence of Ca^{2+}

accumulation by retrograde diffusion around the central cell is hypothesized to affect the frequency of its intracellular calcium oscillations.

In order to explain the mechanism of the retrograde diffusion effect, we introduce the concept of an "effective diffusion coefficient." According to Fick's first law, the flux of Ca^{2+} between two neighboring cells is

$$J = -D_{in} \frac{C_n - C_{n+1}}{\Delta x}, \tag{3-7}$$

where J is the flux of Ca^{2+}; C_n is the calcium concentration of cell n; C_{n+1} is the calcium concentration of cell n+1; D_{in} is the intrinsic diffusion coefficient which is also called the diffusion coefficient in the simulation; and Δx is the intercell spacing. We assume $C_n > C_{n+1}$.

During the propagation process of ICWTs, retrograde diffusion increases C_{n+1} to C_{n+1}^*. We can write the Ca^{2+} flux between cell n and cell n+1 in two ways

$$J = -D_{in} \frac{C_n - C_{n+1}^*}{\Delta x} = -D_{eff} \frac{C_n - C_{n+1}}{\Delta x}, \tag{3-8}$$

where D_{eff} is an effective diffusion coefficient. Because C_{n+1} is less than C_{n+1}^*, D_{in} should be larger than D_{eff}. In the early stages of the propagation of the train of calcium waves (the first 5 pulses), we assume that the retrograde diffusion effect is not large enough to change the oscillation frequency of the stimulated cell. Therefore, the intrinsic diffusion coefficient, D_{in}, can be used as a surrogate for the effective diffusion coefficient when considering the early stages of propagation of calcium waves.

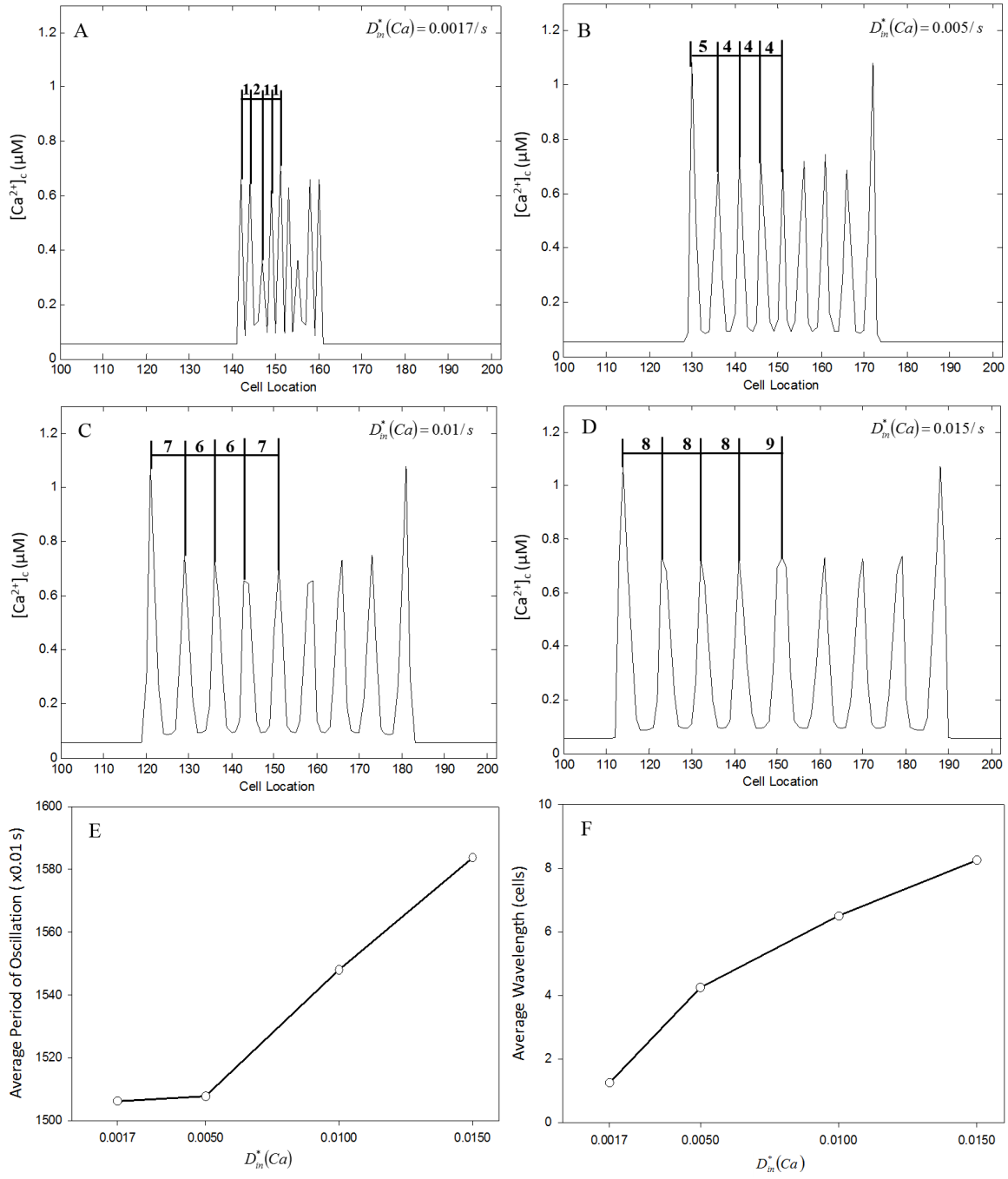

Figure 25. The properties of ICWTs for the different intrinsic calcium diffusion coefficients in the early stage of the ICWTs. (A-D) Early stages of ICWTs for $\boldsymbol{D_{in}^{*}(Ca)}$= 0.0017, 0.005, 0.01, and 0.015 s^{-1}, respectively. The Y-axis represents cytosolic calcium concentrations. The X-axis represents cell locations. (E) The average period of intracellular calcium oscillation of the early stages when $\boldsymbol{D_{in}^{*}(Ca)}$= 0.0017, 0.005, 0.01 and 0.015 s^{-1}, which are represented by the white dots. The Y-axis represents the average period of oscillation. The X-axis represents the intrinsic diffusion coefficient rate of Ca. (F) The average

pulse intervals of the early stages when $\boldsymbol{D^{*}_{in}(Ca)}$= 0.0017, 0.005, 0.01 and 0.015 s^{-1}. The Y-axis represents the average pulse intervals. The X-axis represents the intrinsic diffusion coefficient rate of Ca.

Figure **25** illustrates the properties of ICWTs at the early stage of simulations for different effective (intrinsic) diffusion coefficient rates. Figure **25** *E* shows the variation of oscillation period of the stimulated cell for different values of the diffusion coefficient. When $D^{*}_{in}(Ca)$ is less than 0.0017 s^{-1}, there is no intercellular calcium propagation along the chain. Focusing on $D^{*}_{in}(Ca) \geq 0.0017\,s^{-1}$. When $D^{*}_{in}(Ca)$ is equal to or larger than 0.0017 s^{-1}, the average period of oscillation increases with increasing diffusion coefficient. Figure **25** *F* illustrates the relationship between the effective diffusion coefficient and the average wavelength. This figure shows that the wavelength decreases with a decreasing diffusion coefficient, at least in the early stages of the propagation. This observation can be used to shed light on the decreasing wavelength we reported during the later stage of propagation. Over time the retrograde diffusion process effectively reduces the diffusion flux in the vicinity of the stimulated cell and therefore leads to a reduced effective diffusion coefficient. An effective diffusion coefficient with a value smaller than that of the intrinsic coefficient would result in a shortening of the wavelength.

3.4 Summary

This modeling and simulation study of calcium oscillations and trains of calcium waves in a chain-like cell network is showing that the dynamics of cells embedded in a network is significantly different from that of an isolated cell. In particular we have demonstrated that the transient and steady state frequency of calcium oscillations of a cell stimulated with an agonist depends on its microenvironment, in this case, cell neighbors. This effect is attributed to a crosstalk between the stimulated cell and its environment through retrograde diffusion of calcium

and IP_3. As a growing number of cells in the chain are excited over time and undergo oscillations, retrograde diffusion arising from an expanding train of pulses affects the calcium and IP_3 fluxes in the region that originated the train of waves, that is, in the vicinity of the original stimulated cell. The neighborhood of the stimulated cell forms a "signaling niche" that acts on the stimulated cell itself and affects its dynamics. After stimulation of the single cell, the cellular niche responds to its Ca^{2+} and IP_3 oscillations and signals back through gap-junction mediated diffusion thereby influencing the calcium behavior in the originating cell. This crosstalk leads to a dynamical regulation of the stimulated cell's oscillation frequency. Given the importance in intracellular calcium dynamics in cell function, the niche-dependent changes will likely influence subsequent functions of that single cell. Our simulations always involved the activity of the same, single originating cell and the subsequent impact on calcium behavior throughout the network.

In the tissue space, there will be multiple "originating cells" (meaning more than one cell in the interconnected system is receiving an external activating signal within the same time period), all of which comprise the cellular neighborhood. Thus, the originating cell in one instance is also a potential modifier cell to a neighborhood cell that is originating an oscillation. So, any given cell within a cell neighborhood is both an originating cell and a modifier cell to signals generated elsewhere within the neighborhood. Therefore, the activity of the cell system is greater than the sum of its parts because this type of calcium wave regulation is occurring across the entire system as multiple different cells originate calcium oscillations. Key to this conceptual model is a single-cell centric perspective whereby each cell acts as a signal-originating cell while also populating the cellular niche of other cells within the network. Even though we focused on one originating cell in this study, it should be possible to adapt the computational model to begin to examine this more complex paradigm.

This observation may have striking implications on the role of calcium signaling on cross-level interdependence in multicellular architectures in terms of signal generation and decoding. We have shown that the environment-dependent cross-talk results in Ca^{2+} and IP_3 regulation as well as control over oscillation frequency. Decoding of structural information by individual cells would subsequently need cellular control on frequency dependent intracellular pathways such as frequency-dependent protein phosphorylation by a Ca^{2+} -calmodulin activated kinase which was shown to be ubiquitous in a wide variety of cell types [72]. Therefore, it seems more likely that our calcium-based environment dependent frequency-encoding mechanism is operative in a range of multicellular architectures and tissues.

CHAPTER 4 CONCLUSION AND FUTURE WORK

In this chapter, I briefly summarize the main achievement of this thesis and discuss the possible future work in bio-signal area.

4.1 Conclusion

Calcium wave signal has been found in a wide variety of cell types. Over the last years, a large number of calcium experiments have shown that calcium signal is not only an intracellular regulator but also a long-range signaling. In this thesis, I have studied the propagation of intercellular calcium wave in multicellular structures. Two models was introduced in chapter 2 and chapter 3, respectively.

In chapter 2, the model focuses on the development of an approach with complementary integration of theoretical and experimental methods for studying the multi-level interactions in multicellular architectures and their effect on collective cell dynamic behavior. The fabrication of cell-chain is produced by plasma surface patterning technique. Intercellular calcium waves are induced via mechano-stimuli of selected cells. The experimental observations are complemented by modeling and simulation of calcium wave propagation using a non-linear diffusion/reaction model. Cell-to-cell interactions is considered via intercellular diffusion through gap junctions and described by Fick's second law. The rate of change of intracellular calcium is modeled by a simple calcium dependent non-linear reaction function. Two thresholds are used to determine the value of the calcium release/intake rate. This model suggests that the topology of cell structure will have influence on the competition between intracellular calcium reaction and diffusion, and then control the behavior of intercellular calcium propagation.

Besides mechano-stimulated model, previous studies also mentioned that chemical-stimuli from the extracellular space is able to induce the intracellular calcium oscillation [16,55]. The model in chapter 3 describes the chemical-stimuli based intercellular communication via intracellular calcium/IP_3 oscillations. This model depends on the interdependence between intracellular calcium-IP_3 pathway and cell-cell communication via intercellular diffusion of both Ca^{2+} and IP_3. Different from the mechano-stimuli model, the intracellular dynamic of chemical-stimuli model is based on the IP_3-induced calcium release pathway and formulated into a system of coupled differential equations. To enable the propagation of calcium waves in a one-dimensional chain of cells, we introduce a calcium concentration-dependent threshold-based mechanism to trigger calcium oscillations of individual cells. We investigate the influence of the chain-like multicellular structure on the frequency of calcium oscillations of individual cells. This model shows that after applying an extracellular stimulus, the intracellular oscillation frequency of an individual cell embedded in the chain-like network significantly differs at steady state from that of an isolated cell: the transient behavior of that stimulated cell toward steady oscillations is taking significantly longer in the multicellular network. This behavior is attributed to the retrograde diffusion of Ca^{2+} and IP_3 and highlights the importance of microenvironment on the dynamical behavior of cells in multicellular networks.

In summary, these two models describe new types of higher-order (across structure) behaviors arising from lower-order (within cells) phenomena, and make predictions concerning the mechanisms underlying the dynamics of multicellular biological systems. Microengineered, geometrically constrained networks of human umbilical vein endothelial cells (HUVEC) serve as platforms to arbitrate the theoretical predictions in terms of the effect of network topology on the spatiotemporal characteristics of emerging calcium signals. The theoretical approach describes

numerically the dynamics of non-linear behavior of calcium-based signaling in model networks of cells.

4.2 Future Work

In the mechano-stimuli model, we have introduced the combined experiment and simulation of intercellular calcium wave propagation in the multicellular chain-like and "T" structures. In order to get further understand of calcium propagation, more complex structures should be investigated in both experiment and simulation aspects. Moreover, every cell is considered the same in our model with the same diffusion coefficient. However, it is not always true in experiment. A cell-dependent diffusion coefficient could be introduced to mimic the different diffusion ability of cells.

In chapter 3, we have introduced the theoretical model of chemical-stimuli based intercellular calcium wave propagation in a chain-like structure. The simulation results show that under a certain intracellular oscillation frequency, the intercellular diffusion coefficient has significant influence on the wavelength of intercellular calcium wave trains (ICWTs). However, our further research shows that the value of V_{PLC} and threshold UC may also the significant factors affecting the wavelength of ICWTs. Moreover, more complex multicellular topologies such as "T" structures and "+" structures should be investigated with the objective of studying the relationship between the ICWTs wavelength and calcium transmission rate through the junction area.

From the experiment point of view, a relevant experiment should be established to verify the prediction of the model in chapter 3. The purine receptor agonist ATP could be used as the stimulating agonist and changing the dose the agonist may control the intracellular calcium

oscillation frequency. The usage of Phospholipase C (PLC) inhibitor U-73122 and gap junction inhibitor Carbenoxolone can help to affect the PLC sensitivity and diffusion ability of gap junction, respectively. The experimental results with add of PLC and gap junction inhibitor will enable to test the prediction of significant factors in simulation model in the model.

APPENDIX I: REACTION/DIFFUSION MODEL OF "T" STRUCTURE

Here, we detail the discretized reaction-diffusion equations for the "T" structure illustrated in Figures 10(A) and 13 (A). The reaction-diffusion equations are written for the cells in the junction region, namely cells 30 to 32, cell 1s, cells 1' and 2'. D^* and $D^{*'}$ are the dimensionless diffusion coefficient of edge-to-edge diffusion and vertex-to-vertex diffusion, respectively.

The reaction-diffusion equation for cell 30:

$$C(x_{30},t_{n+1}) = C(x_{30},t_n) + D^*\{[C(x_{31},t_n) - 2C(x_{30},t_n) + C(x_{29},t_n)] + [C(x_{1'},t_n) - C(x_{30},t_n)]\}$$
$$+ D^{*'}[C(x_{1s},t_n) - C(x_{30},t_n)] - k^*(C)C(x_{30},t_n)$$

The reaction-diffusion equation for cell 31 is:

$$C(x_{31},t_{n+1}) = C(x_{31},t_n) + D^*\{[C(x_{32},t_n) - 2C(x_{31},t_n) + C(x_{30},t_n)] + [C(x_{1s},t_n) - C(x_{31},t_n)]\}$$
$$+ D^{*'}\{[C(x_{1'},t_n) - C(x_{31},t_n)] + [C(x_{2'},t_n) - C(x_{31},t_n)]\} - k^*(C)C(x_{31},t_n)$$

The reaction-diffusion equation for cell 32 is:

$$C(x_{32},t_{n+1}) = C(x_{32},t_n) + D^*\{[C(x_{33},t_n) - 2C(x_{32},t_n) + C(x_{31},t_n)] + [C(x_{2'},t_n) - C(x_{32},t_n)]\}$$
$$+ D^{*'}[C(x_{1s},t_n) - C(x_{32},t_n)] - k^*(C)C(x_{32},t_n)$$

The reaction-diffusion equation for cell 1s in side branch is:

$$C(x_{1s},t_{n+1}) = C(x_{1s},t_n) + D^*\{[C(x_{2s},t_n) - 2C(x_{1s},t_n) + C(x_{31},t_n)] + [C(x_{2'},t_n) - 2C(x_{1s},t_n) + C(x_{1'},t_n)]\}$$
$$+ D^{*'}\{[C(x_{32},t_n) - C(x_{1s},t_n)] + [C(x_{30},t_n) - C(x_{1s},t_n)]\} - k^*(C)C(x_{1s},t_n)$$

The reaction-diffusion equation for cell 1' is:

$$C(x_{1'},t_{n+1}) = C(x_{1'},t_n) + D^*[C(x_{1s},t_n) - 2C(x_{1'},t_n) + C(x_{30},t_n)] + D^{*'}[C(x_{31},t_n) - C(x_{1'},t_n)] - k^*(C)C(x_{1'},t_n)$$

The reaction-diffusion equation for cell 2' is:

$$C(x_{2'},t_{n+1}) = C(x_{2'},t_n) + D^*[C(x_{1s},t_n) - 2C(x_{2'},t_n) + C(x_{32},t_n)] + D^{*'}[C(x_{31},t_n) - C(x_{2'},t_n)] - k^*(C)C(x_{2'},t_n)$$

APPENDIX II: FORTRAN CODE OF ICW IN A CHAIN-LIKE MOULTICELLULAR STRUCTURE SUBJECTED TO SINGLE/DOUBLE STIMULATION

```
!CICR simple model
!Propagation is symmetric
!Time- and cell-independent diffusion coefficient
!Parameter values are subjected to change
!Periodic boundary


IMPLICIT NONE
double precision:: rk1, rk2, rk3, rk, coeff, &
uc1, uc2, dt, x, d2c1, b
INTEGER:: nc, nls, nls2, j, jp, jm,i, nt
dimension:: x(801,2), rk(801)
open(unit=1, file='chainS.dat',status='old')
! Just consider 1-D chain

! number of time steps
       print *, "nt="
       read *, nt
!      nt=10000
! number of cells in backbone
       nc=61
! chemical reaction parameter
       rk1=3.0
       rk2=-2.5
       rk3=0.45
! diffusion coeff
       coeff=0.6
! location of stimulation
       nls=21
! Another stimulated cell
!      nls2=41
! critical conc
       uc1=0.3
       uc2=3.0
! time step
       dt=0.01
! inital pulse
       do j=1,nc
       x(j,1)=0.0
       enddo
       x(nls,1)=2.0
!      x(nls2,1)=2.0
! loop of time
       do i=1,nt
! loop over the cells in backbone
       do j=1,nc
       jp=j+1
       jm=j-1
       if(jp>nc)jp=1
       if(jm<1)jm=nc
! reaction
       if(rk(j)==rk3) go to 100
```

```
       if(x(j,1)<=uc1)rk(j)=rk1
       if((x(j,1)<uc2) .and. (x(j,1)>uc1))rk(j)=rk2
       if(x(j,1)>uc2)rk(j)=rk3
100  continue
! diffusion
       d2c1=coeff*(x(jp,1)-2*x(j,1)+x(jm,1))
       x(j,2)=x(j,1)+d2c1*dt-rk(j)*x(j,1)*dt
       enddo
! time shift
       do j=1,nc
       x(j,1)=x(j,2)
       if(j==31) write(1,*) i*dt*2.53, x(j,1)
       enddo
       enddo

   end
```

APPENDIX III: FORTRAN CODE OF ICW IN "T" STRUCTURE SUBJECTED TO SINGLE/DOUBLE STIMULATION

```
!CICR simple model
!Propagation is symmetric
!vertex-to vertex diffusion coefficient is introduced
!Parameter values are subjected to change
!Periodic boundary


IMPLICIT NONE
double precision:: rk1, rk2, rk3, rk, rks, coeff1, &
uc1, uc2, dt, x, xs, d2c1,d2c2,coeff2,xs1,xs2,d2c3,d2c4,rks1,rks2
INTEGER:: nc,nls,ns,k,j,jp,jm,kp,km,i,nt,nlsb,nls2
dimension:: x(601,2), rk(601), rks(300), xs(300,2),xs1(100,2),xs2(100,2),&
       rks1(100),rks2(100)

open(unit=1, file='ST.dat',status='old')
! The simplest complicated structure
! number of time steps
!      print *, "nt="
!      read *, nt
       nt=300
! number of cells in backbone
       nc=61
! number of cells in side branch
       ns=31
! chemical reaction parameter
       rk1=3.0
       rk2=-3.0
       rk3=0.45
! diffusion coeff
       coeff1=0.6
       print *, "coeff2="
       read *, coeff2
! location of side branch
       nlsb=31
! location of stimulation
       nls=28
! Another stimulated cell
!      nls2=34

! critical conc
       uc1=0.3
       uc2=3.0
! time step
       dt=0.01
! inital pulse
       do j=1,nc
       x(j,1)=0
       enddo
       x(nls,1)=2.0
!      x(nls2,1)=2.0
       do j=1,ns
       xs(j,1)=0
       enddo
! loop of time
       do i=1,nt
! loop over the cells in backbone, init
```

```
       do j=2,nc-1
       jp=j+1
       jm=j-1
! reaction
       if(rk(j)==rk3) go to 100
       if(x(j,1)<=uc1)rk(j)=rk1
       if((x(j,1)<=uc2) .and. (x(j,1)>uc1))rk(j)=rk2
       if(x(j,1)>uc2)rk(j)=rk3
100  continue
! diffusion
       if(j==nlsb) then
!cluster model 2---"nlsb" is connecting with xs1 and xs2 and xs(1)
d2c1=coeff1*((x(jp,1)-2*x(j,1)+x(jm,1))+(xs(1,1)-x(j,1)))&
       +coeff2*((xs1(1,1)-x(j,1))+(xs2(1,1)-x(j,1)))

       else if(j==nlsb-1) then
!cluster model 1---"nlsb-1" is connecting with xs(1) and xs1
d2c1=coeff1*((x(jp,1)-2*x(j,1)+x(jm,1))+(xs1(1,1)-x(j,1)))&
       +coeff2*(xs(1,1)-x(j,1))

       else if(j==nlsb+1) then
!cluster model 1---"nlsb+1" is connecting with xs(1) and xs2
d2c1=coeff1*((x(jp,1)-2*x(j,1)+x(jm,1))+(xs2(1,1)-x(j,1)))&
       +coeff2*(xs(1,1)-x(j,1))

       else
       d2c1=coeff1*(x(jp,1)-2*x(j,1)+x(jm,1))
       end if
       x(j,2)=x(j,1)+d2c1*dt-rk(j)*x(j,1)*dt
       enddo

!----------------
! Side Branch
!----------------
       do k=1,ns-1
       kp=k+1
       km=k-1
! reaction
       if(rks(k)==rk3) go to 200
       if(xs(k,1)<=uc1)rks(k)=rk1
       if((xs(k,1)<=uc2) .and. (xs(k,1)>uc1))rks(k)=rk2
       if(xs(k,1)>uc2)rks(k)=rk3
 200  continue

! Diffusion
       if(k==1) then
!connect with cell nlsb, nlsb+1, nlsb-1, xs(1), xs(2),xs1 and xs2
d2c2=coeff1*((xs(kp,1)-xs(k,1))-(xs(k,1)-x(nlsb,1))+(xs2(1,1)-xs(k,1))&
-(xs(k,1)-xs1(1,1)))+coeff2*((x(nlsb-1,1)-xs(k,1))+(x(nlsb+1,1)-xs(k,1)))

       else
       d2c2=coeff1*(xs(kp,1)-2*xs(k,1)+xs(km,1))
       end if
       xs(k,2)=xs(k,1)+d2c2*dt-rks(k)*xs(k,1)*dt
       enddo


!--------------------
! Cluster cells
!--------------------
! reaction
       if(rks1(1)==rk3) go to 300
       if(xs1(1,1)<=uc1)rks1(1)=rk1
```

```
       if((xs1(1,1)<=uc2) .and. (xs1(1,1)>uc1))rks1(1)=rk2
       if(xs1(1,1)>uc2)rks1(1)=rk3
 300  continue
! Diffusion
!connecting with nlsb-1,nlsb and xs(1)
d2c3=coeff1*((xs(1,1)-xs1(1,1))-(xs1(1,1)-x(nlsb-1,1)))&
+coeff2*(x(nlsb,1)-xs1(1,1))

xs1(1,2)=xs1(1,1)+d2c3*dt-rks1(1)*xs1(1,1)*dt

! reaction
       if(rks2(1)==rk3) go to 400
       if(xs2(1,1)<=uc1)rks2(1)=rk1
       if((xs2(1,1)<=uc2) .and. (xs2(1,1)>uc1))rks2(1)=rk2
       if(xs2(1,1)>uc2)rks2(1)=rk3
 400  continue
! Diffusion
! connecting with nlsb+1,nlsb and xs(1)
d2c4=coeff1*((xs(1,1)-xs2(1,1))-(xs2(1,1)-x(nlsb+1,1)))&
+coeff2*(x(nlsb,1)-xs2(1,1))

xs2(1,2)=xs2(1,1)+d2c4*dt-rks2(1)*xs2(1,1)*dt

! time shift in backbone
       do j=1,nc
       x(j,1)=x(j,2)
 if(j==32) write(1,*)i*dt*2.53,x(j,1)
       enddo
! time shift in side branch
       do k=1,ns-1
       xs(k,1)=xs(k,2)
!if(k==4) write(1,*) i*dt*2.53,xs(k,1)
       enddo
! time shift in cluster cells
       xs1(1,1)=xs1(1,2)
       xs2(1,1)=xs2(1,2)
       enddo


!      do j=1,nc
!      write(1,*)j,x(j,1)
!      enddo
!      do k=1,ns-1
!      write(1,*)nc+k,xs(k,1)
!      enddo
!      write(1,*)nc+k+1,xs1(1,1)
!      write(1,*)nc+k+2,xs2(1,1)

end
```

APPENDIX IV: FORTRAN CODE OF CHEMICAL-STIMULATED ICW IN A CHAIN-LIKE MULTICELLULAR STRUCTURE SUBJECTED TO SINGLE STIMULATION

```
!-------------------------------------------------------------------------------------------
--------------
!Politi model (positive)used in calcium propagation in single chain subjected to
single stimulation
!calcium based-vplc controled model
!R-K step size is introduced here.
!periodic boundary condition
!chemical stimulation
!initial concentration keeps the same for each cells
!-------------------------------------------------------------------------------------------
--------------

!-------------------------------------------------------------------------------------------
------------------------
!Thresholds uc1 were introduced
!When Vplc=1.5, max(uc1)=0.067
!D(IP3)=10*D(Ca)
!-------------------------------------------------------------------------------------------
------------------------

! k3k is IP3 phosphorylation rate constant
! k5p is IP3 dephosphorylation rate constant
! kplc is half-activation constant of PLC
! vs is the maximal SERCA pump rate
! k1 is maximal rate of calcium release
! k2 is maximal rate of calcium leak
! ka is calcium binding to activating site
! kp is IP3 binding
! ks half-activation constant
! vplc is the maximal production rate of IP3
! svplc is rescaled maximal PLC activity
! tp is the characteristic time of IP3 turnover
! eta is the ratio of the maxiaml IP3K rate to the total maximal degradation rate of
IP3
! v0 is the constant influx
! fi is the stimulation-dependent influx
! kpm is the half-activation constant
! vpm is the maximal PMCA pump rate
! epsilon is the strength of plasma membrane fluxes
! beta is the ratio of effective volumes ER/cytosol
! tr is the characteristic time IP3R inactivation
! ki is Calcium binding to inhibiting site

IMPLICIT NONE
double precision::fr,uc1,h,c,p,r,tp,k3k,k5p,kplc,vplc,&
       k1,k2,ka,kp,vs,ks,eta,v0,k,ki,ctot,&
       fi,kpm,vpm,svplc,epsilon,beta,tr,&
       temp1IP3,temp1Ca,temp1ER,temp1In,&
       temp2IP3,temp2Ca,temp2ER,temp2In,&
kIP31,tempIP31,kCa1,tempCa1,kER1,tempER1,kIn1,tempIn1,&
kIP32,tempIP32,kCa2,tempCa2,kER2,tempER2,kIn2,tempIn2,&
kIP33,tempIP33,kCa3,tempCa3,kER3,tempER3,kIn3,tempIn3,&
kIP34,kCa4,kER4,kIn4,a,b,d,yu,derivIP3, derivCa, &
```

```
derivER, derivIn,cn,pn,d2Ca,d2IP3,coeffCa,coeffIP3,dt
INTEGER::n,i,j,nc,nls,jm,jp
dimension::c(1000,2),p(1000,2),r(1000),vplc(1000),uc1(1000)

open(unit=1, file='ssppch_Ca.dat',status='old')
open(unit=2, file='ssppch_IP3.dat',status='old')
open(unit=3, file='ssppch_r.dat',status='old')

!-------------------------------------
!      chemical reaction parameter
!-------------------------------------
       kp=0.13
       ks=0.1
       k=0.4
       beta=0.185
       epsilon=0.0
       kpm=0.12
       vpm=0.01
       v0=0.0004
       ctot=2.0
!      print *, "coeffCa="
!      read (*,*)coeffCa
!      print *, "coeffIP3="
!      read (*,*)coeffIP3
       coeffCa=0.005
       coeffIP3=0.05
!------------------------------
!      positive feedback
!------------------------------
       k3k=0.0
       k5p=0.66
       kplc=0.2
       vs=0.9
       fi=0.0047
       k1=1.11
       k2=0.0203
       ka=0.08
       ki=0.4
       tr=12.5
!-------------------------------------
!      number of cells in backbone
!-------------------------------------
       nc=401

!------------------------------
!      location of stimulation
!------------------------------
       nls=201
!---------------------
!      inital pulse
!---------------------
       do j=1,nc
       c(j,1)=0.05
       p(j,1)=0.05
       r(j)=0.85
       enddo
!      c(nls,1)=0.3
!      p(nls,1)=0.3


!-------------------------
!      Threshold
!-------------------------
```

```
       do j=1,nc
       uc1(j)=0.057
       enddo
!-------------------------
!      following vplc
!-------------------------
!      print *, "fr="
!      read (*,*)fr
       fr=1.5
!------------------------
!     time step size
!------------------------
       dt=0.01
!------------------------
!      R-K step size
!------------------------
       h=dt
!--------------------
!      Time Loop
!--------------------
!      print *, "times n="
!      read (*,*)n
n=15000
       do i=1,n

!------------------
!      reaction
!------------------
       do j=1,nc
if(vplc(j)==fr) go to 100
if (j==nls) vplc(j)=fr
if(c(j,1)<uc1(j) .and. j/=nls) vplc(j)=0.0
if(c(j,1)>=uc1(j) .and. j/=nls) vplc(j)=fr
100 continue

!------------------
!Call Subroutine
!------------------
call derivfunction1(c(j,1),p(j,1),vplc(j),derivIP3)
kIP31=h*derivIP3
tempIP31=p(j,1)+0.5*kIP31
!print *,"tempIP31=",tempIP31
call derivfunction2(c(j,1),p(j,1),r(j),vplc(j),derivCa)
kCa1=h*derivCa
tempCa1=c(j,1)+0.5*kCa1
!print *,"kCa1=",kCa1
!print *,"tempCa1=",tempCa1
call derivfunction3(c(j,1),r(j),derivIn)
kIn1=h*derivIn
tempIn1=r(j)+0.5*kIn1
!print *,"tempIn1=",tempIn1

call derivfunction1(tempCa1,tempIP31,vplc(j),derivIP3)
kIP32=h*derivIP3
tempIP32=p(j,1)+0.5*kIP32
!print *,"tempIP32=",tempIP32
call derivfunction2(tempCa1,tempIP31,&
tempIn1,vplc(j),derivCa)
kCa2=h*derivCa
tempCa2=c(j,1)+0.5*kCa2
!print *,"kCa2=",kCa2
!print *,"tempCa2=",tempCa2
call derivfunction3(tempCa1,tempIn1,derivIn)
```

```
kIn2=h*derivIn
tempIn2=r(j)+0.5*kIn2
!print *,"tempIn2=",tempIn2

call derivfunction1(tempCa2,tempIP32,vplc(j),derivIP3)
kIP33=h*derivIP3
tempIP33=p(j,1)+kIP33
!print *,"tempIP33=",tempIP33
call derivfunction2(tempCa2,tempIP32,&
tempIn2,vplc(j),derivCa)
kCa3=h*derivCa
tempCa3=c(j,1)+kCa3
!print *,"kCa3=",kCa3
!print *,"tempCa3=",tempCa3
call derivfunction3(tempCa2,tempIn2,derivIn)
kIn3=h*derivIn
tempIn3=r(j)+kIn3
!print *,"tempIn3=",tempIn3

call derivfunction1(tempCa3,tempIP33,vplc(j),derivIP3)
kIP34=h*derivIP3
!print *,"kIP34=",kIP34
call derivfunction2(tempCa3,tempIP33,&
tempIn3,vplc(j),derivCa)
kCa4=h*derivCa
!print *,"kCa4=",kCa4
call derivfunction3(tempCa3,tempIn3,derivIn)
kIn4=h*derivIn
!print *,"kIn4=",kIn4

p(j,2)=p(j,1)+(kIP31+2.0*(kIP32+kIP33)+kIP34)/6.0
c(j,2)=c(j,1)+(kCa1+2.0*(kCa2+kCa3)+kCa4)/6.0
r(j)=r(j)+(kIn1+2.0*(kIn2+kIn3)+kIn4)/6.0
!if(j==nls-2)write(3,*)i,r(j)
enddo


!-----------------------------------------------------
!Diffusion---loop over the cells in backbone, init
!-----------------------------------------------------
       do j=1,nc
       jp=j+1
       jm=j-1
       if(jp>nc)jp=1
       if(jm<1)jm=nc
d2Ca=coeffCa*(c(jp,1)-2*c(j,1)+c(jm,1))
!if(j==nls)write(1,*)i,d2Ca
d2IP3=coeffIP3*(p(jp,1)-2*p(j,1)+p(jm,1))
!if(i==10 .and. j==20) print *,"d2IP3=", d2IP3
c(j,2)=c(j,2)+d2Ca*dt
p(j,2)=p(j,2)+d2IP3*dt

       enddo
!------------------------
!      Time shift
!------------------------
       do j=1,nc
       c(j,1)=c(j,2)
       p(j,1)=p(j,2)
if(j==nls-2)write(1,*)i,c(j,1)
if(j==nls-3)write(2,*)i,p(j,1)
       enddo
!if(j==nls-12)write(1,*)i,vplc(j)
```

```
!if(j==nls-12)write(3,*)i,uc1(j)
! write(1,*)i
!write(2,*)i
!write(3,*)i
       do j=1,nc
!      write(1,*)j,c(j,1)
!      write(2,*)j,p(j,1)
!      write(3,*)j,r(j)
       end do

!-----------------------------
!      end of time loop
!-----------------------------
       enddo

end

subroutine derivfunction1(c,p,vplc,derivIP3)
double precision, intent(out)::derivIP3
double precision, intent(in):: c,p,vplc
double precision:: tp,k3k,k5p,kplc,&
eta,k,ki,svplc,a,b,d
!positive feedback
       k=0.4
       k3k=0.0
       k5p=0.66
       kplc=0.2
tp=1.0/(k5p+k3k)
!print *, "tp=",tp
eta=k3k/(k3k+k5p)
!print *, eta
svplc=vplc*tp
!print *, "svplc=",svplc
!a=svplc*c**2
!print *, "a=",a
!b=kplc**2+c**2
!print *, "b=",b
!d=(eta*c**2)/(k**2+c**2)
!print *, "d=",d
derivIP3=(((svplc*c**2)/(kplc**2+c**2))&
-((eta*c**2)/(k**2+c**2)+(1-eta))*p)/tp
!print *,"derivIP3=",derivIP3
return
end subroutine derivfunction1

subroutine derivfunction2(c,p,r,vplc,derivCa)
double precision, intent(out)::derivCa
double precision, intent(in):: c,p,r,vplc
real:: tp,k3k,k5p,kplc,&
k1,k2,ka,kp,vs,ks,eta,v0,k,ki,fi,kpm,&
vpm,svplc,epsilon,beta,tr,e,f,g,h,ctot
       kp=0.13
       ks=0.1
       k=0.4
       epsilon=0.0
       kpm=0.12
       vpm=0.01
       v0=0.0004
       ctot=2.0
       beta=0.185
!positive feedback
       k3k=0.0
```

```
       k5p=0.66
       kplc=0.2
       vs=0.9
       fi=0.0047
       k1=1.11
       k2=0.0203
       ka=0.08
tp=1.0/(k5p+k3k)
svplc=vplc*tp
derivCa=(k1*((r*c*p)/((ka+c)*(kp+p)))**3+k2)*(((ctot-c)/beta)-c)&
-((vs*c**2)/(ks**2+c**2))&
+epsilon*(v0+(fi*svplc)-((vpm*c**2)/(kpm**2+c**2)))
!print *, "derivCa=",derivCa
return
end subroutine derivfunction2


subroutine derivfunction3(c,r,derivIn)
double precision, intent(out)::derivIn
double precision, intent(in):: c,r
real:: tp,k3k,k5p,kplc,vplc,&
       k1,k2,ka,kp,vs,ks,eta,v0,k,ki,&
       fi,kpm,vpm,svplc,epsilon,beta,tr,j
!      positive feedback
       ki=0.4
       tr=12.5
!j=1-r*(ki+c)/ki
!print *, "j=",j
derivIn=(1-r*(ki+c)/ki)/tr
!print *, "derivIn=",derivIn
return
end subroutine derivfunction3
```

APPENDIX V: MATLABE CODE FOR ANALYZING THE BEHAVIOR OF INTERCELLULAR CALCIUM WAVE TRAINS

```
function [ output_args ] = timepoint( FileName )
%Analyze the ICWTs including the pulse interval, peak and trough value of
%pulses

[x,y,z]=textread(FileName);% import data into matlab
data=zeros(36000,1);
time=zeros(35,1);
conc=zeros(301,1);
peak=zeros(35,1);
intv=zeros(25,1);
j=0;
% Find the time point when the calcium level in stimulated cell reaches the
% highest level.
for i=[1:36000]
    data(i,1)=y((152)+(i-1)*302);%calcium concentration of stimualted cell as
function of time
end
for i=[2:35999]
    if data(i,1)>data(i-1,1) && data(i,1)>data(i+1,1)
        j=j+1;
        time(j,1)=i;
    end
end
%time(j)=0;
disp(time);
%Find the location of each pulse at some particular time points
for j=[1:35]
    if time(j)~=0
        conc=y((2:302)+(time(j)-1)*302);
        c=0;
        m=0;
        for k=[2:151]
            if conc(k)>conc(k-1) && conc(k)>conc(k+1)
                c=c+1;
                peak(c)=k;
            end
        end
        disp(peak);
        %Calculate the pulse interval
        for c=[1:35]
            if peak(c)~=0
            m=m+1;
            intv(m)=peak(c+1)-peak(c)-1;
                if intv(m)<0
                intv(m)=0;
                end
            end
        end
        disp(intv);
```

```
    end
end


end
```

APPENDIX VI: MATLABE CODE FOR MAKING THE SNAPSHOT OF INTERCELLULAR CALCIUM WAVE TRAINS

```
function [ output_args ] = FigurePlot( FileName,FolderName )
%FIGUREPLOT Summary of this function goes here
%Code for making snapshot

[x,y,z]=textread(FileName);
data=zeros(301,1);
for i=34988:34990
data(:,1)=y((2:302)+(i-1)*302);
plot((1:301),data,'-k');
 axis([1 301 0.0 1.3]);
%set(gca, 'XTick',[20 60 90 120 150 180 210 240 280]);
%set(gca, 'XTickLabel',{'30','60','90','120','150','180','210','240','270'});
%data=y((31:73)+(i-1)*102);
%axis([20 282 0.0 1.3]);
xlabel('Cell Location');
 ylabel('[Ca](uM)');
%hleg1=legend('T=32379');
 if (i<10)
 saveas(gcf,strcat(FolderName,'0000',int2str(i),'file.jpg'));
 end;
 if ((i<100) && (i>=10))
 saveas(gcf,strcat(FolderName,'000',int2str(i),'file.jpg'));
 end;
 if ((i<1000) && (i>=100))
%if (i==509)
 saveas(gcf,strcat(FolderName,'00',int2str(i),'file.tif'));
end;
 if ((i<10000) && (i>=1000))
%if (i==6317)
saveas(gcf,strcat(FolderName,'0',int2str(i),'file.tif'));
end;
 if ((i<100000) && (i>=10000))
%if ((i==11563) || (i==16616) || (i==19125) || (i==24138))
%if (i==34989)
saveas(gcf,strcat(FolderName,int2str(i),'.tif'));
%print -r1000;
end;
output_args=0;
end
end
```

REFERENCE

1. Berridge, M. J., F. R.S., P. H. Cobbold and K. S. R. Cuthbertson. 1988. Spatial and Temporal Aspects of Cell Signalling. *Philosophical Transactions-Royal Society. Biological Sciences.* 320:325-343

2. Tyler, A. 1941. Artificial parthenogenesis. *Biol. Rev. Camb. Philos. Soc.* 16:291-336.

3. Ozil, J. P., B. Banrezes, S. Toth, H. Pan and R. Schultz, 2006. Ca^{2+} oscillatory pattern in fertilized mouse eggs affects gene expression and development to term. *Developmental Biology.* 300:534-544

4. Bissell, M. J., A. Rizki and I. S. Mian. 2003. Tissue architecture: the ultimate regulator of breast epithelial function. *Current Opinions in Cell Biology*. 15:753-762

5. Kirshner, J., C. J. Chen, P. Liu, J. Huang and J. E. Shively. 2003. CEACAM1-4S, a cell-cell adhesion molecule, mediates apoptosis and reverts mammary carcinoma cells to a normal morphogenic phenotype in a 3D culture. *Proc. Natl. Acad. Sci. USA.* 100:521-526

6. Ridgeway, E. B., J. C. Gilkey and L. F. Jaffe. 1977. Free calcium increases explosively in activating medaka eggs. Proc. *Nati. Acad. Sci. USA.* 74: 623-627

7. Thomas, A. P., G. S. Bird, G. Hajnóczky, *et al.* 1996. Spatial and temporal aspects of cellular calcium signaling. *FASEB J.* 10: 1505-1517

8. Berridge, M. J. 1990. Calcium oscillations. *J. Biol. Chem.* 17: 9583-9586

9. Gray, P. T. A. 1988. Oscillations of free cytosolic calcium evoked by cholinergic and catecholaminergic agonists in rat parotid acinar cells. *J. Physiol*. 6: 715-760

10. Yule, D. I. and D. V. Gallacher. 1988. Oscillations of cytosolic calcium in single pancreatic acinar cells stimulated by acetylcholine. *FEBS Lett*. 239:358-362

11. Jacob, R. J. E., Merritt, T. J. Hallam and T. J. Rink. 1988. Repetitive spikes in cytoplasmic calcium evoked by histamine in human ehdothelial cells. *Nature*. 335: 40-45

12. Malgaroli, A., R. Fesce and J. Meldolesi. 1990. Spontaneous $[Ca^{2+}]_i$ fluctuations in rat chromaffin cells do not require inositol 1,4,5-trisphosphate elevations but are generated by a caffeine- and ryanodine-sensitive intracellular Ca^{2+} store. *J. Biol. Chem*. 265: 3005-3008

13. Berridge, M. J. and A. Galione. 1988. Cytosolic calcium oscillators. FASEB. J. 2:3074-82

14. Cuthbertson, K. S. R. and T. R. Chay. 1991. Modelling Receptor-Controlled Intracellular Calcium Oscillators. *Cell Calcium*. 12:97-109

15. Woodring, P. J. and J. C. Garrison. 1997. Expression, Prufication, and Regulation of Two Isoforms of The Inositol-1,4,5-trisphosphate 3-kinase. *J. Biol. Chem*. 272:30447-30454

16. Meyer, T. and L. Stryer. 1991. Calcium Spiking. *Annu. Rev. Biophys. Biophys. Chem*. 20:153-74

17. Meyer, T. and L. Stryer. 1988. Melecular model for receptor-stimulated calcium spiking. *Proc. Natl. Acad. Sci. USA*. 85: 5051-5055

18. Goldbeter, A., G. Dupont, and M. J. Berridge. 1989. Minimal model for signal-induced Ca^{2+} oscillations and for their frequency encoding through protein phosphorylation. *Proc. Natl. Acad. Sci. USA*. 87: 1461-1465

19. Berridge, M. J. 1991. Cytoplasmic calcium oscillations: A two pool model. *Cell Calcium*. 12: 63-72

20. Sanderson, M. J. and E. R. Dirksen. 1985. A Versatile And Quantitative Computer-Assisted Photoelectronic Technique Used For The Analysis of Ciliary Beat Cycles. Cell Motil. 5: 267-292

21. Sanderson, M. J. and E. R. Dirksen. 1988. Fura-2 Fluorescence Reveals That Intercellular Communication Elevates Intracellular Calcium in Tracheal Ciliated Cells. *Biolys*. 53: A52

22. Girard, P. R. and J. R. Kennedy. 1986. Calcium Regulation of Ciliary Activity in Rabbit Tracheal Epithelial Explants and Outgrowth. *Eur. J. Cell Biol*. 40: 203-209

23. Sanderson, M. J. and E. R. Dirksen. 1989. Mechanosensitivity and Beta-Adrenergic Control of The Ciliary Beat Frequency of Mammalian Respiratory Tract Cells in Culture. Am. Rev. Respir. Dis. 139: 432-440.

24. Sanderson, M. J., A. C. Charles, S. Boitano and E. R. Dirksen. 1994. Mechanisms and Function of Intercellular Calcium Signaling. *Molecular and Cellular Endocrinology*. 98:173-187

25. Sanderson, M. J., A. C. Charles and E. R. Dirksen. 1990. Mechanical Stimulation and Intercellular Communication Increases Intracellular Ca^{2+} In Epithelia Cells. *Cell Regul.* 1: 585-596.

26. Finkbeiner, S. 1992. Calcium Waves in Astrocytes-Filling in The Gaps. *Neuron*. 8:1101-1108

27. Xia, S. L. and J. Ferrier. 1992. Propagation of A Calcium Pulse Between Osteoblastic Cells. *Biochem. Biophys. Res. Commun*. 186:1212-1219

28. Drumheller, P. D and J. A. Hubbell. 1991. Local Modulation of Intracellular Calcium Levels Near A Single-Cell Wound in Human Endothelial Monolayers. *Arteriol. Thromb*. 11: 1258-1265

29. Bennett, M .V. L. and V. K. Verselis. 1992. Biophysics of Gap Junctions. Sem. Cell Biol. 3:29-47

30. Saez, J. C., J. A. Connor, D. C. Spray and M. V. L. Bennett. 1989. Hepatocyte Gap Junctions Are Permeable To The Second Messenger, Inositol-1,4,5-trisphosphate, And To Calcium Ions. Proc. Natl. Acad. Science. 86: 2708-2712.

31. Sneyd, J., A. C. Charles and M. J. Sanderson. 1994. A Model for The Propagation of Intercellular Calcium Waves. *American Journal of Physiology---Cell Physiology*. 266: C293-C302

32. Hofer, T., L. Venance and C. Giaume. 2002. Control and Plasticity of Intercellular Calcium Waves in Astrocytes: A Modeling Approach. *J. Neurosci.* 22: 4850–4859

33. Bellinger, S. 2004. Modeling calcium wave oscillations in astrocytes. *Neurocomputing*. 65–66: 843–850

34. Bagher, P. and S. S. Segal. 2011. Regulation of Blood Flow In the Microcirculation: Role of Conducted Vasodilation. Acta Physiol 202: 271-284

35. Hansen, R. K. and M. J. Bissell. 2000. Tissue architecture and breast cancer: The role of extracellular matrix and steroid hormones. *Endocrine-Related Cancer* 7: 95-113

36. Davidson L. A. 2008. Integrating morphogenesis with underlying mechanics and cell biology. *Curr Top Dev Biol*. 81: 113-133

37. Tran, Q. K., K. Ohashi, H. Watanabe. 2000. Calcium signaling in endothelial cells. *Cardiovascular Research*. 48: 13-22

38. Watts, D. J., S. Strogatz. 1998. Collective dynamic of "small-world" networks. *Nature*. 393: 440-442

39. Eray, M., P. A. Deymier, J. B. Hoying, K. Runge and J. O. Vasseur. 2008. Resonant filtering of compositional waves in multicellular networks. *Physica D*. 237: 2777

40. Deymier, P. A., M. Eray, J. B. Hoying, K. Runge and J. O. Vasseur. 2010. Architecture-dependent signal conduction in model networks of endothelial cells. *Phys Rev E Stat Nonlin Soft Matter Phys*. 81: 041915

41. Deymier, P. A., J. B. Hoying, K. Runge and J. O. Vasseur. 2010. Calcium wave propagation in chains of endothelial cells with non-linear reaction dynamics: green's function approach. *Phys Rev E*. 82: 041913

42. Ali, M. H. and P. T. Schumacker. 2002. Endothelial Responses to Mechanical Stress: Where Is The Mechanosensor? *Crit Care Med* 30: S198-S206

43. Junkin, M, S. L. Leung, S. Whitman, C. C. Gregorio and P. K. Wong. 2011. Cellular self-organization via autocatalytic alignment feedback. *J Cell Sci*. 124: 4213-4220.

44. Junkin, M and P. K. Wong. 2011. Probing cell migration in confined environments by plasma lithography. *Biomaterials*. 32: 1848-1855

45. Keyes, J., M. Junkin, J. Cappello, X. Wu and P. K. Wong. 2008. Evaporation-induced assembly of biomimetic polypeptides. *Appl Phys Lett*. 93: (023120)1-(023120)3

46. Junkin, M., J. Watson, J. P. Vande Geest, P. K. Wong. 2009. Template-guided self-assembly of colloidal quantum dots using plasma lithography. *Adv Mater*. 21:1247-1251

47. Junkin, M., S. L. Leung, Y. Yang, Y. Lu, J. Volmering, P. K. Wong. 2011. Plasma Lithography Surface Patterning For Creation of Cell Networks. *J Vis Exp*. 14(52). pii: 3115. doi: 10.3791/3115

48. Bezprozvanny, I., J. Watras and B. E. Ehrlich. 1991. Bell-shaped calcium-response curves of IP3 and calcium-gated channels from endoplasmic reticulum of cerebellum. *Nature*. 351: 751-754

49. Meissner, G. 1994. Ryanodine receptor/Ca^{2+} release channels and their regulation by endogenous effectors. *Annu Rev Physiol*. 56: 485—508

50. Combettes, G. L. and L. Leybaert. 2007. Calcium dynamics: spatio-temporal organization from the subcellular to the organ level. *Int Rev Cytol*. 261: 193–245

51. Finch, E. A., T. J. Turner and S. M. Goldin. 1991. Calcium as a coagonist of inositol 1,4,5-trisphosphate-induced calcium release. *Science.* 252: 443-446

52. Bagher, P., M. J. Davis and S. S. Segal. 2011. Visualizing Calcium Responses to Acetylcholine Convection Along Endothelium of Arteriolar Networks in Cx40BAC-GCaMP2 Transgenic Mice. *Am J Physiol Heart Circ Physiol*. 301: H794-802

53. Allbritton, N. L., T. Meyer and L. Stryer. 1992. Range of Messenger Action of Calcium Ion and Inositol 1,4,5-Trisphosphate. *Science*. 258: 1812-1815

54. Dupont, G, M. J. Berridge and A. Goldbeter. 1991. Signal-Induced Ca^{2+} Oscillations: Properties of A Model Based On Ca2"-Induced Ca^{2+} Release. *Cell Calcium.* 12:73-86.

55. Gracheva, M. E., and J. D. Gunton. 2003. Intercellular communication via intracellular calcium oscillation. *J. Theor. Biol*. 221: 513-518

56. Rooney, T., E. Sass and A. P. Thomas. 1989. Characterization of cytosolic calcium oscillations induced by phenylephrine and vasopressin in single fura-2-loaded hepatocytes. *J. Biol. Chem.* 264: 17131-17414

57. Goldberg, M., M. De Pitta, V. Volman, H. Berry, and E. Ben-Jacob. 2010. Nonlinear gap junctions enable long-distance propagation of pulsating calcium waves in astrocytes networks. *PloS Computational Biology*. 6:e1000909

58. Lacar, B., S. Z. Young, J. C. Platel and A. Bordey. 2011. Gap junction-mediated calcium waves define communication networks among murine postnatal neural progenitor cells. *Eur. J. Neurosci*. 34:1895

59. Dani, J. W., A. Chernjavsky and S. J. Smith. Neuronal activity triggers calcium waves in hippocampal astrocyte networks. *Neuron*. 8:429-40

60. Malmersjo, S., P. Rebellato, E. Smedler, H. Planert, P. Uhlen, et al. 2013. Neural progenitors organize in small-world networks to promote cell proliferation. *PNAS*. 110:E1524

61. Othmer, H. G. and L. E. Scriven. 1971. Instability and dynamic pattern in cellular networks. *J. Theor. Biol.* 32:507-537

62. Turing A. M. 1952. The chemical basis of morphogenesis. *Philosophical Transactions of the Royal Society of London, Series B, Biological Sciences*. 237:37-72

63. Dobrzynski, L. and H. Puszkarski. 1989. Eigenvectors of composite systems. I. General theory. *Journal of Physics: Condensed Matter.* 1:1239-1245

64. Long, J., M. Junkin, PK. Wong, J. B. Hoying, and P.A. Deymier. 2012. Calcium wave propagation in networks of endothelial cells: model-based theoretical and experimental study. *PloS Comput Bio.* 8:e1002847

65. Politi, A., L. D. Gaspers, A. P. Thomas, and T. Hofer. 2006. Models of IP_3 and Ca^{2+} oscillations: Frequency encoding and identification of underlying feedbacks. *Biophysical Journal*. 90:3120-3133

66. Rhee, S. G. 2001. Regulation of phosphoinositide-specific phosphoplipase C. *Annu. Rev. Biochem.* 70:281-312

67. Harootunian, A. T., J. P. Kao, S. Parajape, and R. Y. Tsien. 1991. Generation of calcium oscillations in fibroblasts by positive feedback between calcium and IP3. *Science*. 251:75-78

68. Verkhratsky, A., R. K. Orkand, and H. Kettenmann. 1998. Glial calcium: homeostasis and signaling function. *Physiol. Rev.* 78: 99–141

69. Communi, D., V. Vanweyenberg, and C. Erneux. 1997. D-myo-inositol-1,4,5-trisphosphate 3-kinase A is activated by receptor activation trough a calcium: Calmodulin-dependent protein kinase II phosphorylation mechanism. *EMBO J.* 16:1943-1952

70. Berridge, M. J. 1993. Inositol trisphosphate and calcium signaling. *Nature*. 361:315-325

71. Gaspers, L. D., A. P. Thomas. 2005. Calcium signaling in liver. *Cell Calcium*. 38: 329–342

72. Koninck, P. De, and H. Schulman. 1998. Sensitivity of Ca^{2+}/calmodulin-dependent protein kinase II to the frequency of Ca oscillations. *Science*. 279:227